European Cells and Materials Vol. 46 2023 (pages 57-90) DOI: 10.22203/eCM.v046a04 ISSN 1473-2262

NOTOCHORDAL CELL-DERIVED MATRIX INHIBITS MAPK SIGNALING IN THE DEGENERATIVE DISC ENVIRONMENT

L.T. Laagland[1,§], F.C. Bach[1,§], F.M. Riemers[1], G. Erdmann[2], T.S. Braun[3], G.G.H. van den Akker[4], T.C. Schmitz[5], L.B. Creemers[6], C. Sachse[2], C.L. Le Maitre[7], T.J.M. Welting[4,8], K. Ito[5,6], M.F. Templin[3] and M.A. Tryfonidou[1,*]

[1] Department of Clinical Sciences, Faculty of Veterinary Medicine, Utrecht University, Utrecht, The Netherlands
[2] NMI TT Pharmaservices, Berlin, Germany
[3] NMI Natural and Medical Sciences Institute at the University of Tübingen, Reutlingen, Germany
[4] Laboratory for Experimental Orthopedics, Department of Orthopedic Surgery, Maastricht University, Maastricht, The Netherlands
[5] Orthopaedic Biomechanics, Department of Biomedical Engineering, Eindhoven University of Technology, Eindhoven, The Netherlands
[6] Department of Orthopedics, University Medical Centre Utrecht, Utrecht, The Netherlands
[7] Department of Oncology and Metabolism, Medical School, The University of Sheffield, Sheffield, UK
[8] Laboratory for Experimental Orthopedics, Department of Orthopedic Surgery, Maastricht University Medical Centre+, Maastricht, The Netherlands
[§] These authors contributed equally

Abstract

Chronic low back pain is often caused by intervertebral disc (IVD) degeneration. Preceding this degenerative process, the main cellular phenotype in the nucleus pulposus shifts from notochordal cells (NCs) to nucleus pulposus cells (NPCs). In previous studies, porcine NC-derived matrix (NCM), containing NC-secreted factors, induced matrix anabolic effects and inhibited pro-inflammatory mediators in NPCs *in vitro* and in degenerated canine IVDs *in vivo*. As the underlying mechanisms remained elusive, this study aimed to explore this with targeted gene expression and proteomic (DigiWest technology) analysis focused on inflammatory signaling pathways.

After 6 hours, NCM (10 mg/mL) treatment initially stimulated pro-inflammatory mediators in canine and human NPCs *in vitro* and increased signaling in a chondrosarcoma derived Nuclear factor-κB reporter cell line. At protein level, NCM mainly induced changes in the Mitogen-activated protein kinase (MAPK) pathway after 72 hours. Expression of inhibitory Dual-specificity phosphatase (DUSP) proteins was increased in NCM-treated NPCs, whereas the expression of the three main pillars of the MAPK pathway (extracellular signal-regulated kinase (ERK)/cJun N-terminal kinase (JNK)/protein kinase C (PKC)) was inhibited. In follow-up validation, *in vivo* degenerated canine IVDs treated with an intradiscal NCM injection demonstrated increased DUSP5 and healthy nucleus pulposus marker (cytokeratin 19, Paired box 1 (PAX1), Forkhead Box F1 (FOXF1)) immunopositivity after 6 months of treatment.

Altogether, NCM initially stimulated pro-inflammatory mediators *in vitro*, but thereafter exerts its prolonged effects by inhibiting the MAPK pathway. These findings provide insights in the underlying mechanisms involved in the instructive capacity of this naturally-derived biomaterial with the potential to serve as a cell-free NC-based therapy to treat intervertebral disc degeneration.

Keywords: Intervertebral disc degeneration, inflammation, notochordal cells, extracellular matrix, mitogen-activated protein kinase pathway, dual specificity phosphatase.

***Address for correspondence**: Marianna A. Tryfonidou, Prof. dr. H. Jakobgebouw, Yalelaan 108, 3584 CM Utrecht, The Netherlands
Telephone number: +31 30 253 4558 Email: m.a.tryfonidou@uu.nl

Copyright policy: This article is distributed in accordance with Creative Commons Attribution Licence (http://creativecommons.org/licenses/by/4.0/).

List of Abbreviations

ADAMTS	Disintegrins and metalloproteinases with thrombospondin motifs
AF	Annulus fibrosis
AFI	Average fluorescence intensity
AGE	Advanced glycation end products
ANOVA	Analysis of variance
Asap	Ascorbic acid 2-phosphate
BMP	Bone Morphogenetic Proteins
BSA	Bovine serum albumin
CA12	Carbonic Anhydrase 12
CDC	cyclin-dependent kinase
cNPC	Canine nucleus pulposus cell
DUSP	Dual-specificity phosphatase
ECM	Extracellular matrix
ERK	Extracellular signal-regulated kinase
EP	Endplate
FBS	Fetal bovine serum
FDR	False Discovery Rate
FGF	Fibroblast growth factor
FOXF1	Forkhead Box F1
GAPDH	Glyceraldehyde 3-phosphate dehydrogenase
hNPC	Human nucleus pulposus cell
HSA	Human serum albumin
IL	Interleukin
IL-1R	Interleukin-1 receptor
IVD	Intervertebral disc
JAK2	Janus Kinase 2
JNK	cJun N-terminal kinase
KRT	Cytokeratin
NC	Notochordal cell
NP	Nucleus pulposus
NPC	Nucleus pulposus cell
LBP	Low back pain
MAPK	Mitogen-activated protein kinase
MMP	Metalloproteinase
MSC	Mesenchymal stromal cell
NCM	Notochordal cell-derived matrix
NF-κB	Nuclear factor-κB
P	Phosphorylated
PAX1	Paired box protein
PBS	Phosphate-Buffered Saline
PBST	Phosphate-Buffered Saline + Tween
PGE2	Prostaglandin E2
PKC	Protein kinase C
P/S	Penicillin/Streptomycin
RT-qPCR	Reverse transcription-quantitative polymerase chain reaction
S6	S6 ribosomal protein
SPRED2	Sprouty Related EVH1 Domain Containing 2
TNF	Tumor Necrosis Factor

Introduction

Low back pain (LBP) is a major health and socioeconomic problem throughout the world, and its incidence is rising due to ageing of the human population (Clark and Horton, 2018). Degeneration of the intervertebral disc (IVD) is a common cause for chronic LBP (Freemont, 2009). Current treatments for chronic LBP are only symptomatic, and include physiotherapy, analgesic medication (*e.g.* Non-Steroidal Anti-Inflammatory Drugs, opioids), and eventually surgery. Therefore, there is an urgent need for minimally invasive (regenerative) strategies that promote biological IVD repair (Bach *et al*., 2022).

During IVD degeneration, the activity of catabolic enzymes such as matrix metalloproteinases (MMPs) and disintegrins and metalloproteinases with thrombospondin motifs (ADAMTS) increases under the influence of locally produced inflammatory cytokines, *e.g.* interleukin-1β (IL-1β) (Le Maitre *et al*., 2005) and Tumor Necrosis Factor (TNF) (Wang *et al*., 2017a). Pathways that are known to play a role in this catabolic process in the degenerated IVD include inflammatory signaling pathways, *e.g.* Mitogen-activated protein kinase (MAPK) and its downstream Nuclear factor-κB (NF-κB) signaling (Daniels *et al*., 2017; Mi *et al*., 2018; Ni *et al*., 2019). Altogether, these changes lead to a loss of healthy extracellular matrix (ECM) and decreased structural integrity of the IVD. Because of abovementioned events, the normal function of the IVD deteriorates, which leads to a vicious circle, since the IVD becomes more vulnerable to damage under loading (Vergroesen *et al*., 2015).

In the young and healthy IVD, large vacuolated notochordal cells (NCs) are present in the nucleus pulposus (NP) (Hunter *et al*., 2004). These cells disappear, while smaller chondrocyte-like nucleus pulposus cells (NPCs) appear during maturation and ageing in several species that spontaneously develop chronic LBP due to IVD degeneration, including humans and dogs (Bach *et al*., 2022). Previous work has already demonstrated that NC-secreted biomolecular factors evoke anabolic responses in various cell/tissue types, such as mesenchymal stromal cells (MSCs), annulus fibrosus (AF) cells, endplate (EP) chondrocytes, NPCs, NP explants and *in vivo* rat IVDs (for all studies, see (Bach *et al*., 2022)). Thus, NC-based treatment strategies for IVD degeneration leading to chronic LBP, appear to be promising.

In an attempt to exploit the instructive capacity of the specialized NC matrix as a cell-free treatment approach, porcine NC-derived matrix (NCM) from healthy NC-rich NP tissue, as a first step towards clinical translation was previously used (Bach *et al*., 2018). NCM, containing ECM and biologic factors secreted by NCs, may act rather comparable to demineralized bone matrix, which contains ECM and growth factor components (*e.g.* Bone Morphogenetic Proteins (BMPs) (Pietrzak *et al*., 2012)) native to bone and is employed in clinical practice for bone healing (Gruskin *et al*., 2012). Porcine NCM induced an anabolic response in bovine NPCs and inhibited *TNFα* and *IL-1β* expression *in vitro* (Schmitz *et al*., 2022; de Vries *et al*., 2019). These effects seemed to be tissue dependent, as NCM induced more potent anabolic effects compared to bovine-derived NP matrix (*i.e.* NP tissue devoid of NCs), while the latter stimulated deposition of collagen type I typically present in degenerative fibrotic processes (de Vries et al., 2018b). Moreover, NCM also induced *in vitro* and *in vivo* ECM anabolic effects on degenerated canine IVDs and inhibited the gene expression of inflammatory cytokines (*IL-1β* and *TNF*), production of Prostaglandin E2 (PGE2), and the accumulation of advanced glycation end products (AGEs) evidenced by the brown discoloration of tissue (Bach *et al*., 2018).

Despite the abovementioned promising observations, the underlying mechanism behind the anabolic effects of NCM on IVD cells remains elusive. Therefore, the aim of this study was to determine the mode of action of porcine NCM in the degenerative IVD environment. Insights into the mechanism will allow for a better understanding of the underlying biology and contribute to the development of NC-based therapeutic approaches.

Materials and Methods

Experimental setup

To explore the underlying mechanisms of NCM, this study examined its effects, thereby focusing on cell phenotype and inflammatory signaling pathways that could potentially be involved in NCM's catabolic and anabolic mechanisms. For this purpose, canine and human NPCs (both species that spontaneously develop IVD

degeneration and LBP (Bach *et al*., 2022)) were cultured in monolayer with and without NCM. After 6, 24, and 72 hours, reverse transcription-quantitative polymerase chain reaction (RT-qPCR) was performed on inflammatory markers. To confirm short term inflammatory-like responses, an NF-κB reporter chondrosarcoma cell line (Neefjes *et al*., 2021) was incubated with and without NCM for 6 hours. After 72 hours, protein was collected from cultured NPCs and targeted proteomics was performed using DigiWest technology (Treindl *et al*., 2016) to determine which pathways were activated by NCM. Furthermore, results were confirmed at tissue level in mildly and moderately degenerated *in vivo* canine IVDs treated with NCM (immunohistochemistry for specific proteins identified with DigiWest; Dual-specificity phosphatase 5 (DUSP5), (phosphorylated) extracellular signal-regulated kinase ((p-) ERK), and cytokeratin 19 (KRT-19)) and specific proteins of interest (interleukin-1β (IL-1β), interleukin-1 receptor I (IL-1R), Forkhead Box F1 (FOXF1), and Paired box protein 1 (PAX1)) (Fig. 1).

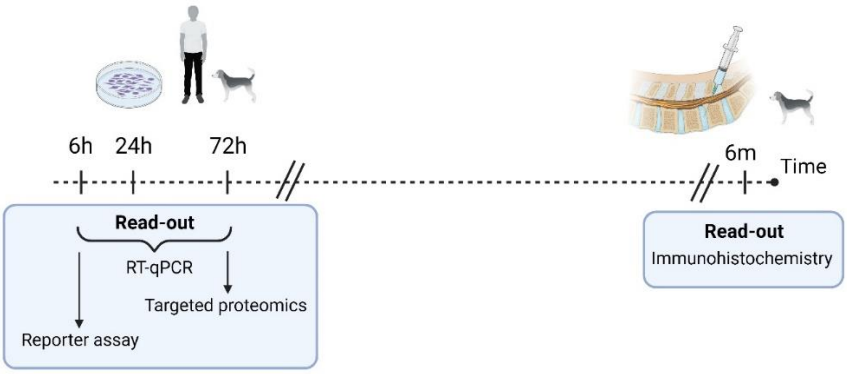

Fig. 1. Experimental setup. Human and canine nucleus pulposus cells (NPCs) from degenerated IVDs were cultured for 6, 24, and 72 hours in monolayers with and without porcine-derived NCM (10 mg/mL). At each timepoint, samples were collected for RT-qPCR and after 72 hours also for targeted proteomics. Additionally, a chondrosarcoma cell-derived NK-κB reporter cell line was cultured with and without 10 mg/mL NCM for 6 hours. Results were confirmed with immunohistochemistry of mildly and moderately degenerated dog IVDs 6 months after intradiscal injection with either no, 1× or 2× 10 mg/mL NCM (Bach *et al*., 2018).

Table 1. Details of the canine and human donors used in the cell culture experiments. Canine nucleus pulposus cells (NPCs) were obtained from all IVDs, whereas the human NPCs were obtained from the lumbar part of the spine.

Number	Age (years)	Passage	Gender	Breed	Thompson grade
Canine donors					
C1	5	P2	Female	Beagle	2/3 (mild degeneration)
C2	5	P2	Female	Beagle	2/3 (mild degeneration)
C3	6	P2	Male	Beagle	2/3 (mild degeneration)
C4	2	P2	Male	Beagle	2/3 (mild degeneration)
Human donors					
H1	38	P3	Female	N/A	3 (mild degeneration)
H2	58	P3	Female	N/A	3 (mild degeneration)
H3	50	P3	Male	N/A	3 (mild degeneration)
H4	44	P3	Male	N/A	3 (mild degeneration)

NCM generation

Thompson score I, healthy NP tissue was collected from complete spines (all levels) of 3-month-old porcine donors from the slaughterhouse in accordance with local regulations (permit number 457642.09). Previous

research has shown that this NP tissue is rich in NCs (Bach *et al*., 2015; Bach *et al*., 2022) based on morphology and expression of common NC-markers (Williams *et al*., 2023). To produce NCM, the NP tissue was lyophilized overnight, pulverized into a fine powder with a microdismembrator (Sartorius, Goettingen, Germany) and resuspended at 10 mg/mL in hgDMEM + Glutamax (31966, Thermo Fisher Scientific, Waltham, MA, USA). Furthermore, NCM was supplemented with 1 % Penicillin/Streptomycin (P/S) (P11-010, GE Healthcare Life Sciences, Boston, MA, USA), 1 % ITS+ premix (354352, Corning Life Sciences, Corning, NY, USA), 0.04 mg/mL L-proline (P5607, Sigma-Aldrich, St. Louis, MO, USA), 0.1 mM Ascorbic acid 2-phosphate (Asap; A8960, Sigma-Aldrich, Darmstadt, Germany), and 1.25 mg/mL Human Serum Albumin (HSA; Albumax, Sanquin Plasma Products, Amsterdam, The Netherlands), additives that are also included in basal culture medium (Bach *et al*., 2018). NCM generation and concentration were based on our previous study (Bach *et al*., 2018).

Cell culture and protein isolation

Complete spines were collected from Beagles (chondrodystrophic dog breed) that had been euthanized in unrelated research studies (approved by the Utrecht University Animal Ethics Committee; Centrale Commissie Dierproeven, Table 1). IVDs from human donors (Table 1) were obtained during a standard *postmortem* diagnostic procedure in which part of the lumbar spine was collected within 48 hours after death, as approved the Local Medical Ethical Committee number (12-364). The material was used in line with the code 'Proper Secondary Use of Human Tissue' as installed by the Federation of Biomedical Scientific Societies. IVDs were opened under sterile conditions and NP tissue was collected by precise separation from AF and EPs (Bach *et al*., 2015).

The NPCs were expanded at 5 % O_2, 5 % CO_2, 37 °C until passage 2 (canine) or 3 (human) in expansion medium (Bach *et al*., 2015) containing hgDMEM + Glutamax with 10 % FBS (Gibco 10500-064, Thermo Fisher Scientific, Waltham, MA, USA), 1 % P/S, 0.1 mM Asap, and 1 ng/mL fibroblast growth factor (FGF) (PHP105, AbD Serotec, Raleigh, NC, USA) in 60 mm dishes (150462, ThermoFisher, Waltham, MA, USA). Medium was changed twice weekly. When the NPCs reached 80 % confluence, FBS free basal medium was added for 48 hours after which the experiment started. After the monolayers were washed with Hank' Balanced Salt solution (Gibco 14025, Thermo Fisher Scientific, Waltham, MA, USA), the NPCs received control (basal) culture medium or NCM (basal medium with 10 mg/mL NCM). Basal culture medium consisted of hgDMEM + Glutamax with 1 % P/S, 1 % ITS+ premix, 0.04 mg/mL L-proline, 0.1 mM Asap, and 1.25 mg/mL HSA (Bach *et al*., 2015). After 6, 24, and 72 hours, samples were collected for RNA isolation, cDNA synthesis and RT-qPCR, as described previously (Bach *et al*., 2015) for the inflammation-related genes given in Table 2. The CT values were normalized for the average CT values of the four reference genes. Furthermore, a chondrosarcoma derived NF-κB reporter cell line (Neefjes *et al*., 2021) was used. This is a nanoluciferase reporter construct with the NFκB-RE sequence inserted. Then lentiviral particles (Takara Lenti-X: Takara Bio, Kusatsu, Shiga, Japan) were generated and transduced into SW1353 cells. For this experiment, cells were seeded at 67,000 cells/well in a 384 well-format (Greiner Bio-One, Frickenhausen, Germany) in DMEM/F12 + 0.5 % FBS, 1 % P/S for 24 hours. Next, the cells were cultured for 6 hours in basal medium with and without 10 mg/mL NCM (generated from 3 different 3-month-old porcine donors). Finally, the luciferase signal was measured with NanoGlo reagents using a Tristar 2 multimode reader (Berthold, Bad Wildbad, Germany).

For targeted proteomic analysis, NPCs were washed after 72 hours, twice with ice cold Phosphate-Buffered Saline (PBS) and protein was collected by scraping. Protein was collected in 10-30 μL PBS in Eppendorf Protein LoBind tubes (Z666505, Sigma-Aldrich, St. Louis, MO, USA) until further analysis. Provided that NCM stimulated deposition of its ECM components within 72 hours, interfering components were removed with a 2D clean-up kit (80648451, GE Healthcare, Boston, MA, USA) according to the manufacturer's instructions.

Table 2. Primers used for quantitative PCR of canine and human samples. All primers were designed in-house using Perlprimer. Bp: base pairs.

Canine genes	Forward sequence 5′ → 3′	Reverse sequence 5′ → 3′	Amplicon size (bp)	Annealing temp (°C)	Accession no.
Reference genes					
GAPDH	TGTCCCCACCCCCAATGTATC	CTCCGATGCCTGCTTCACTACCTT	100	58	NM_001003142
HPRT	AGCTTGCTGGTGAAAAGGAC	TTATAGTCAAGGGCATATCC	104	58	NM_001003357
RPS19	CCTTCCTCAAAAAGTCTGGG	GTTCTCATCGTAGGGAGCAAG	95	61	XM_005616513
SDHA	GCCTTGGATCTCTTGATGGA	TTCTTGGCTCTTATGCGATG	92	56.5	XM_535807
Target genes					
IL-1ß	TGCTGCCAAGACCTGAACCAC	TCCAAAGCTACAATGACTGACACG	115	68	NM_001037971
IL-6	GAGCCCACCAGGAACGAAAGAGA	CCGGGGTAGGGAAAGCAGTAGC	123	65	NM_001003301
IL-8	CTGTTGCTCTCTTGGCAGC	GGGATGGAAAGGTGTGGAG	122	63.5	XM_850481
COX2	TTCCAGACGAGCAGGCTAAT	GCAGCTCTGGGTCAAACTTC	112	60	NM_001003354
TNF	CCCCGGGCTCCAGAAGGTG	GCAGCAGGCAGAAGAGTGTGGTG	83	65	NM_001003244
Human genes					
Reference genes					
HPRT	TATTGTAATGACCAGTCAACAG	GGTCCTTTTCACCAGCAAG	192	60	NM_000194.2
SDHA	TGGGAACAAGAGGGCATCTG	CCACCACTGCATCAAATTCATG	86	58	NM_004168.3
TBP	TGCACAGGAGCCAAGAGTGAA	CACATCACAGCTCCCCACCA	132	63.5	NM_003194.4
YWHAZ	ACTTTTGGTACATTGTGGCTTCAA	CCGCCAGGACAAACCAGTAT	94	64	NM_003406.3
Target genes					
IL-1ß	CCCTAAACAGATGAAGTGCTCCTT	GTAGCTGGATGCCGCCAT	67	60	NM_000576
IL-6	TCGAGCCCACCGGGAACGAA	GCAGGGAAGGCAGCAGGCAA	136	60	NM_000600
IL-8	CAAGAGCCAGGAAGAAACCA	TCTAAGTTCTTTAGCACTCCTTGG	148	63.5	NM_000584
COX2	GGGAACACAACAGAGTATGC	TCTCCTATCAGTATTAGCCTGC	97	59.5	NM_000963
TNF	GCCGCATCGCCGTCTCCTAC	AGCGCTGAGTCGGTCACCCT	121	61.5	NM_000594

DigiWest technology and data analysis

Targeted proteomics was performed on 4.5 ± 0.7 μg (canine) and 9 μg (human) protein per sample with DigiWest® (Reutlingen, Germany), a proprietary immunoassay technology which transfers Western Blot to a high-throughput bead-based microarray platform (Treindl *et al*., 2016). In short, the proteins in each sample were separated by gel electrophoresis (NuPAGE® Novex® 4-12% Bis-Trisprotein gel, 1.0 mm, 12 well, 150 V, 90 min), blotted onto a polyvinylidene difluoride membrane (30 V, 75 min) and biotinylated (one hour), followed by a Ponceau staining. After one wash with Phosphate-Buffered Saline + Tween (PBST) and drying overnight, the lanes were then cut into 96 strips to generate different molecular weight fractions, and the proteins on the strips were eluted in 96-well plates (Greiner Bio-One, Frickenhausen, Germany). After protein elution in 10 μL 8 M Urea in 100 mM Tris-HCl pH 9.5 including 1 % Triton-X100, neutravidin coated, color-coded MagPlex beads (Luminex, Austin, TX, USA) were added to the proteins. After overnight-coupling, leftover coupling sites were blocked with the use of deactivated NHS-PEG12-biotin (500 μM, 1 h). Beads were pooled and the original Western Blot lanes reconstructed by reassigning the color IDs of the MagPlex beads to the molecular weight fraction.

DigiWest beads were blocked in assay buffer (ELISA blocking reagent, Roche, Rotkreuz, Switzerland) supplemented with 0.2 % milk powder, 0.05 % Tween-20, 0.02 % sodium azide) in a 96-well plate (Corning, NY, USA). Beads were incubated in 30 μL primary antibody (**Supplementary File 1**) at 15 °C overnight. After washing twice with PBST, R-Phycoerythrin-conjugated secondary antibody was added for 1 h at 23 °C. Beads were then washed twice with PBST and readout was performed on a Luminex PlexMAP 3D instrument (Treindl *et al*., 2016).

For peak identification and quantification of the antibody specific signals, the DigiWest analysis tool was employed. This tool uses the 96 values for each initial lane obtained from the Luminex measurements on the 96 molecular weight fractions, this identifies the peaks at the appropriate molecular weight, calculates a baseline using the local background, and integrates the peaks. The reported values present the peak specific fluorescence intensity (AFI, accumulated fluorescence intensity) (Treindl *et al*., 2016).

For the canine samples, a total of 237 antibodies for NP phenotypic markers and proteins involved in inflammatory signaling pathways plus species-specific blanks and protein loading controls were employed (**Supplementary File 1**). For some antibodies, no protein was detected resulting in 71 (canine) and 49 (human) remaining antibodies that were used for further analysis. For these antibodies, the signals were filtered to exclude proteins that were undetectable in the majority of the samples by employing. The cut-off value of > 400 average fluorescence intensity (AFI) was calculated as follow: nSamples*baseline + ngroups*baseline (to enable transformation, all signals below detection limit were arbitrarily assigned a baseline value of 33 AFI). Applying this filter, at the cut-off value of 400 AFI, removed 14 of the 71 antibodies leaving 57 antibodies (canine) and removed 7 of the 49 antibodies leaving 42 antibodies (human) for further analysis.

Analysis of the DigiWest data was conducted in R-Studio (v1.1), R (v3.4.4), Bioconductor 2.3. Scaling and normalization was conducted group-wise based on the streptavidin signal and visualized with multidimensional scaling. Differential protein expression patterns (log2 fold-change; log2FC) were obtained using pairwise exactTests using edgeR (v3.20.9) followed by *posthoc* False Discovery Rate (FDR) correction according to the Benjamini and Hochberg's method to calculate the adjusted p-values. Thereafter, the significantly differentially expressed proteins were further analysed using "toppgene" and subsequently, a Panther overrepresentation test using the Reactome, pathways as the annotation data set was performed. For the antibodies producing multiple bands, the summed values over the bands were used and the individual single band values removed.

Immunohistochemical staining of (NCM-treated) canine IVDs

In a previous study, the effect of 10 mg/mL NCM was determined on degenerated canine IVDs *in*

vivo (*n* = 5 Beagles) (Bach *et al*., 2018). Briefly, 50 µL of NCM was intradiscally injected in mildly (spontaneously; no NX-IVDs) and moderately (induced by partial NP removal; NX-IVDs) degenerated canine IVDs. After three months, NCM was reinjected in a moderately and mildly degenerated IVD (2× NCM) to determine whether multiple injections would exert a more beneficial effect than a single injection. Six months after the first injections, IVDs were collected for histological purposes. The spinal units (½ vertebra – EP – IVD – EP – ½ vertebra) were sagittally transected and the samples were fixed in 4 % buffered formaldehyde for 14 days, decalcified in PBS with 0.5 M Ethylenediaminetetraacetic acid for two months and embedded in paraffin (Bach *et al*., 2018).

The histological samples (control, 1× NCM, 2× NCM, all from mildly and moderately degenerated IVDs) were included in the current study to determine the effect of NCM on protein immunopositivity *in vivo* (Table 3). For this purpose, 5-µm sections were mounted on Microscope KP+ slides (KP-3056, Klinipath, Duiven, The Netherlands) and deparaffinized through xylene (two times 5 minutes) and graded ethanol (100 %, 96 %, 70 %; two times 5 minutes each), followed by one PBS rinse. The sections were blocked for 10 minutes with 0.3 % H_2O_2 in PBS and washed two times for 5 minutes with PBS + 0.1 % Tween (PBST 0.1 %). If needed, antigen retrieval was performed (Table 3). Thereafter, sections were blocked for 30 minutes with 5 % bovine serum albumin (BSA; A3095, Sigma-Aldrich, St. Louis, MO, USA) in PBS and incubated overnight at 4 °C with the primary antibody in 5 % BSA in PBS and negative control IgGs (Table 3). The negative controls (Table 3) showed no specific staining. The next day, the sections were washed with PBST 0.1 % before the secondary antibody (in similar concentration as primary antibody) was applied for 60 minutes at room temperature (Table 3). After washing with PBS, the sections were incubated with the liquid 3,3'-diaminobenzidine substrate chromogen system (K3468, Dako, Denmark) for 2 minutes and counterstained with Mayers hematoxylin (1.09249.0500, Merck, Darmstadt, Germany) for one minute. Thereafter, they were washed with tap water for 10 minutes and dehydrated with graded ethanol (70 %, 96 %, 100 %) and xylene (two times 5 minutes each) and mounted with Pertex (00811-EX, Histolab, Sweden).

Table 3. Details of the immunohistochemistry protocols. *: DUSP5 antibody specifically only detects DUSP5, no other DUSP variants.

Target protein	Primary ab	Secondary ab	Antigen retrieval	Negative control
Aggrecan (ACAN)	Mouse monoclonal Recombinant Anti-Aggrecan antibody [6-B-4] (ab3778) 48 µg/mL	EnVision+ System-HRP Goat Anti-Mouse (K4001, Dako)	Pronase (1 mg/mL, 60 min), followed by Hyaluronidase (10 mg/mL, 60 min)	AffiniPure Fab Fragment Goat Anti-Mouse IgG (115-007-003, Jackson Immunoresearch) 48 ug/mL
Extracellular signal-regulated kinase 1 (ERK1)	Mouse monoclonal Anti-ERK 1 Antibody (G-8): sc-271269 4 µg/mL	EnVision+ System-HRP Goat Anti-Mouse (K4001, Dako)	None	AffiniPure Fab Fragment Goat Anti-Mouse IgG (115-007-003, Jackson Immunoresearch) 4 µg/mL
Phosphorylated ERK 1/2 (pERK1/2)	pERK rabbit polyclonal antibody (9101, Cell Signaling Technology) 1.9 µg/mL	EnVision+ System-HRP Goat-anti-Rabbit (K4002, Dako)	Citrate buffer (10 mM, pH 6, 30 min, 70 °C)	Anti-Rabbit IgG (HAF008, R&D Systems) 1.9 µg/mL

*Dual-specificity phosphatase 5 (DUSP5)**	DUSP5 mouse monoclonal antibody (clone 2F3, H00001847-M04, Novus Biologicals) 0.18 μg/mL	EnVision+ System-HRP Goat Anti-Mouse (K4001, Dako)	None	AffiniPure Fab Fragment Goat Anti-Mouse IgG (115-007-003, Jackson 0.18 μg/mL
Interleukin-1β (IL-1β)	Mouse monoclonal anti-IL-1 beta antibody [OTI3E1] (ab156791) 40 μg/mL	EnVision+ System-HRP Goat Anti-Mouse (K4001, Dako)	None	AffiniPure Fab Fragment Goat Anti-Mouse IgG (115-007-003, Jackson 40 μg/mL
Interleukin – 1 receptor IL-1R	IL1R1 Monoclonal Antibody (MA1-10858, Thermofisher) 18 μg/mL	M EnVision+ System-HRP Goat Anti-Mouse (K4001, Dako)	None	AffiniPure Fab Fragment Goat Anti-Mouse IgG (115-007-003, Jackson 18 μg/mL
Paired box protein 1 (PAX1)	Rabbit polyclonal anti-PAX1 antibody (ab203065) 20 μg/mL	Goat-anti-Rabbit (K4002, Dako)	Citrate buffer (10 mM, pH 6, 30 min, 70 °C)	Anti-Rabbit IgG (HAF008, R&D Systems).
Forkhead Box F1 (FOXF1)	Recombinant Anti-FOXF1 antibody (ab168383) 13.8 μg/mL	Goat-anti-Rabbit (K4002, Dako)	Citrate buffer (10 mM, pH 6, 30 min, 70 °C)	Anti-Rabbit IgG (HAF008, R&D Systems).
Cytokeratin 19 (KRT19)	Anti-Cytokeratin 19 mouse monoclonal antibody [RKRT108] (ab9221) 40 μg/mL	EnVision+ System-HRP Goat Anti-Mouse (K4001, Dako)	None	AffiniPure Fab Fragment Goat Anti-Mouse IgG (115-007-003, Jackson 40 μg/mL

Raw images of the NP region (two per NP) were captured with a Leica DFC420C digital camera (Leica Microsystems, Amsterdam, The Netherlands) mounted to a BX60 microscope (Olympus, Leiderdorp, The Netherlands) and Leica Application Suite (V4.2) software package. All positively and negatively stained cells were manually counted (nuclear and cytoplasmatic staining). Adobe Photoshop CC 2017 18.1.0 (San Jose, California, USA) was used to manually count (positively stained) cell numbers in two randomly selected NP areas per IVD section as described previously (Bach *et al*., 2016b). The mean percentage of cells that stained positive over the total number of cells present (ratio) was determined for every target protein. Immunopositivity thus indicates ratio of positive cells, not intensity of the staining.

Statistical analysis

Statistical analyses on the RT-qPCR and immunohistochemical data were performed using IBM SPSS Statistics 24 (IBM Corp., Armonk, NY, USA). Normal distribution was tested with the Shapiro-Wilk test. If data were normally distributed, a one-way analysis of variance (ANOVA) was used, while if data were not normally distributed, a Mann-Whitney U test was performed. Because multiple samples didn't show any immunopositivity, for the KRT19 immunohistochemical data of the *in vivo* study a Chi-Square test was performed. The one-way ANOVA and Mann-Whitney U tests were

followed by a Benjamini Hochberg *post-hoc* test to correct for multiple comparisons. *p*-values < 0.05 were considered as statistically significant.

Results

NCM induces an initial inflammatory response

Gene expression analysis was performed on canine (cNPCs) and human NPCs (hNPCs) from degenerated IVDs cultured for 6, 24, and 72 hours in monolayers with or without 10 mg/mL NCM. *IL-1β* and *TNF* mRNAs were not detected at any time point. NCM induced *IL-8* expression in cNPCs and *IL-6* expression in hNPCs after 6 hours of treatment, but not at later time points (Fig. 2**b,d**). *IL-6* expression was not detected in cNPCs (Fig. 2**a**) and IL-8 expression was not significantly affected by NCM treatment in hNPCs (Fig. 2**e**). *COX2* expression was increased by NCM in cNPCs after 6 and 24 hours and in hNPCs after 6, 24 and 72 hours of treatment (Fig. 2**c,f**). Furthermore, increased NF-κB signaling activity was detected in the reporter cell line by its exposure to NCM derived from 3 individual porcine donors (Fig. 2**g**).

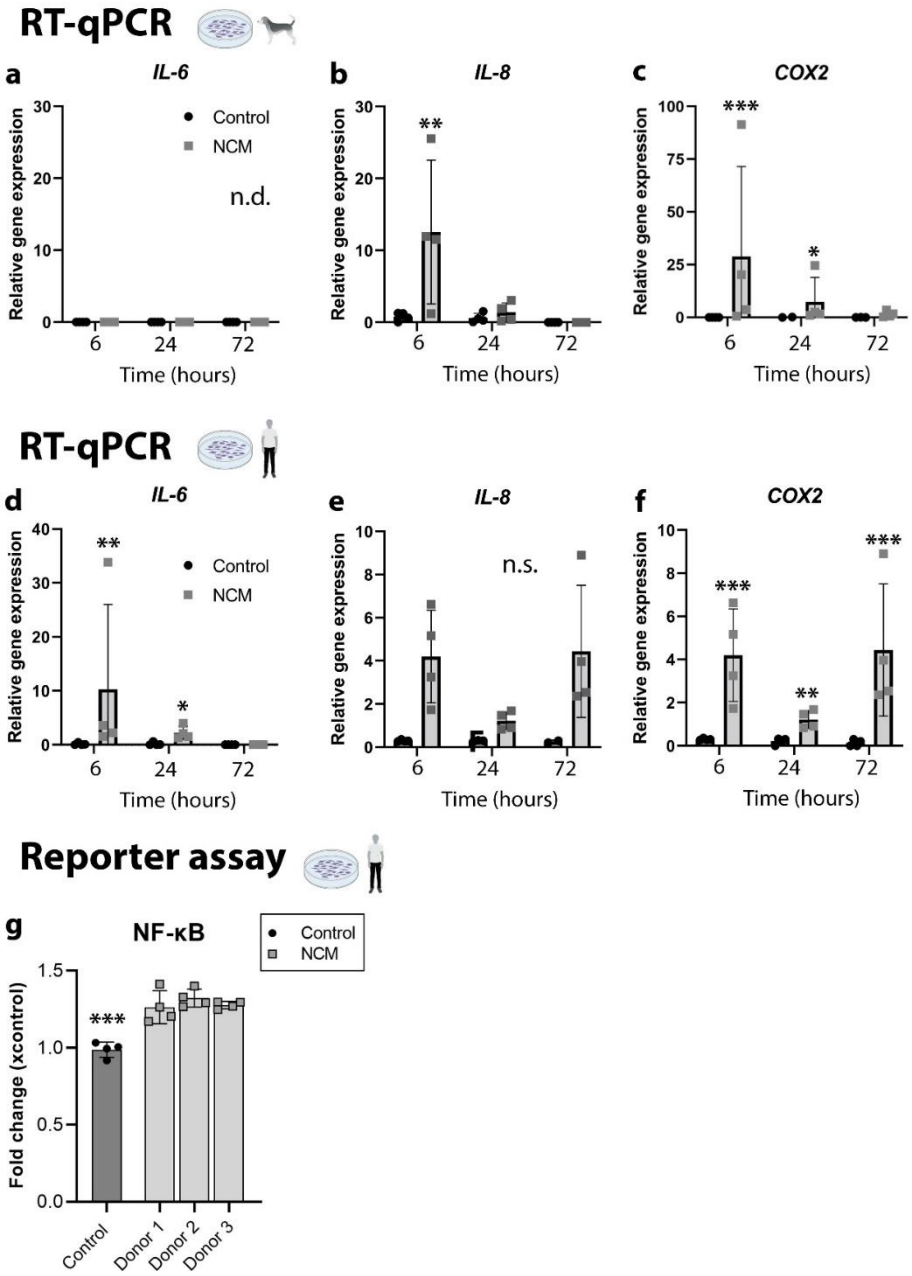

Fig. 2. NCM induces an initial inflammatory response in human and canine NPCs. Relative gene expression ($E^{\Delta\Delta CT}$) of canine NPCs for (**a**) *IL-6*, (**b**) *IL8*, (**c**) *COX2* and human NPCs for (**d**) *IL-6*, (**e**) *IL-8*, and (**f**) *COX2* after 6, 24, and 72 hours monolayer culture with basal culture medium with/without 10 mg/mL NCM. Log10 scale is used for the y-axis, *n*=4. (**g**) n-Fold change (x control) of induction of an NF-κB chondrosarcoma reporter cell line after 6 hours of culture with basal culture medium with/without 10 mg/mL NCM of 3 different porcine donors measured in quadruplicate. IL: interleukin, COX2: cyclo-oxygenase 2. *, **, ***: $p < 0.05$, 0.01, and < 0.001 respectively. n.s.: not significantly affected. n.d.: not detected.

NCM affects multiple signaling pathways

Targeted proteomic analysis showed that several pathways were affected by NCM treatment both *in vitro* and *in vivo*, which results are discussed in more detail below. Additional pathways that were affected in canine and human NPCs are included in Table 4 and 5 respectively.

NCM inhibits the MAPK pathway

DigiWest analysis showed that 72 hours of NCM treatment significantly induced the expression of proteins that are known to dephosphorylate the Mitogen-activated protein kinase (MAPK) key signaling molecules, *e.g.* Dual-Specificity Phosphatase (DUSP) 5 and 6 in cNPCs ($p \leq 0.05$, Fig. 3**c,d**). In contrast, DUSP16 expression was decreased ($p < 0.01$, Fig. 3**f**) in cNPCs while DUSP9 and DUSP1 were not significantly affected and the active phosphorylated (p) form of DUSP1 not detected (Fig. 3**a**,**b,e**). In hNPCs, expression of pDUSP1 as well as DUSP5 was induced by NCM ($p < 0.001$, Fig. 3**g,i**), whereas unphosphorylated DUSP1 was significantly decreased ($p < 0.001$, Fig. 3**h**). DUSP6 was not detected and DUSP9 and DUSP16 were not significantly affected in hNPCS (Fig. 3**j,k,l**). Since NCM induced DUSP5 expression in both hNPCs and cNPCs, DUSP5 immunopositivity was determined in degenerated canine IVDs treated with NCM *in vivo* (Bach *et al*., 2018). Confirming the DigiWest results, canine IVDs treated with 2× NCM demonstrated increased DUSP5 immunopositivity compared with control and 1× NCM IVDs, in both mildly (no NX-IVDs) or moderately degenerated discs (NX-IVDs) ($p < 0.05$, Fig. 3**m,n**).

Fig. 4 depicts tables and volcano plots for top proteins differentially expressed in 72 hours NCM-treated cNPCs (Fig. 4**a**) and hNPCs (Fig. 4**b**) versus controls, as determined by DigiWest technology.

MAPK signaling proteins are evolutionarily conserved serine/threonine kinases, which regulate signal transduction and cell responses, *i.e.* cell proliferation, differentiation, survival, death, and inflammation. An overview of all significantly up/downregulated proteins in the MAPK pathway by NCM treatment is given in Fig. 5 (Cargnello and Roux, 2011; Chen *et al*., 2019; Fenton and Gout, 2011; Huang and Tan, 2012; Li *et al*., 2016; Nakashima, 2002; Nishina *et al*., 2004; Lopez-Bergami P *et al*., 2007). Generally, the expression of proteins upstream in the MAPK pathway (*e.g.* RAS, MAP2K, MAP3K, p38) were not significantly affected in hNPCs and cNPCs treated with NCM compared with controls (Fig. 5). In hNPCs, but not in cNPCs, however, NCM decreased the expression of p-RAF (Fig. 5) and Mitogen-activated protein kinase kinase kinase kinase 1 (MAP4K1; $p < 0.001$, Fig. 6**l**). The expression of key proteins further downstream the MAPK pathway were also mostly inhibited by NCM, such as p-extracellular signal-regulated kinase 1/2 (p-ERK1/2, $p < 0.05$, Fig. 6**a,g**), p-c-Jun N-terminal kinase/stress-activated protein kinase (p-JNK/SAPK, $p < 0.001$, Fig. 6**f**), and p-protein kinase C (p-PKC, $p < 0.01$, Fig. 6**c,i**), while p-S6 ribosomal protein (p-S6) expression was increased ($p < 0.01$, Fig. 6**e,k**) in cNPCs and hNPCs. A difference between cNPCs and hNPCs was encountered in the expression of (p-)c-Jun; this protein was upregulated in cNPCs, but downregulated in hNPCs by NCM ($p < 0.001$, Fig. 6**d,j**). Furthermore, ERK1/2 expression was significantly increased by NCM in hNPCs, but not affected in cNPCs (Fig. 6**b**,**h**). Reactome pathway analysis also indicated that the MAPK (sub)pathways (*e.g.* Sprouty, FGF) were regulated by NCM (Table 4 and 5). In the canine IVDs that were treated with 2× NCM *in vivo*, ERK1 immunopositivity was significantly higher compared with controls after 6 months ($p = 0.05$,

Fig. 6**m,n**), while p-ERK1/2 immunopositivity was absent in all conditions (data not shown). Additionally, immunopositivity for IL-1β and IL-1R was not different between any condition (Fig. 7).

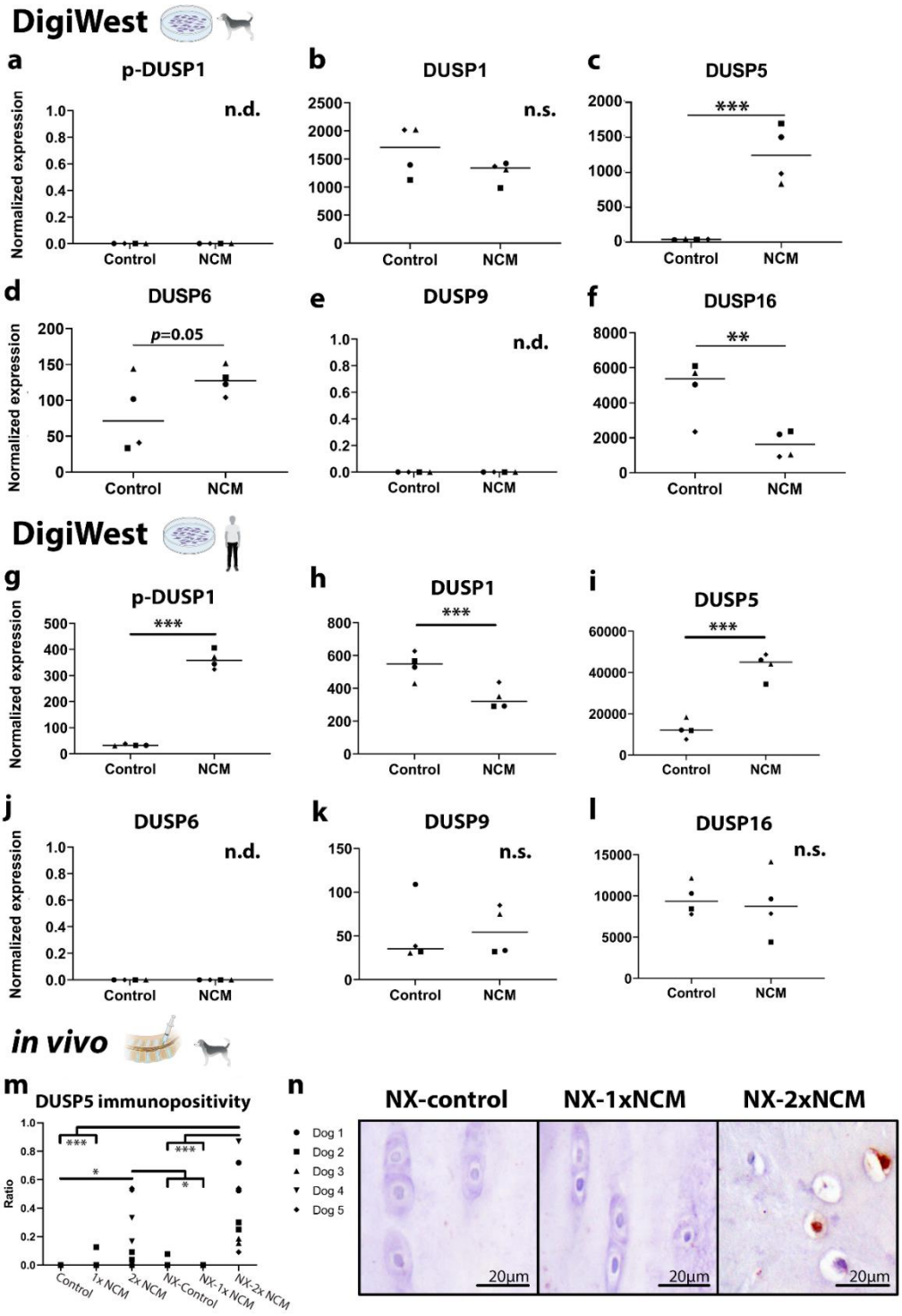

Fig. 3. NCM affects Dual-Specificity Phosphatase (DUSP) expression in canine and human NCM-treated NPCs versus controls, as determined by DigiWest technology and in degenerated canine IVDs treated with NCM *in vivo*. (**a-l**) Canine and human NPCs were treated for 3 days with basal culture medium with/without 10 mg/mL NCM. **: $p < 0.01$, ***: $p < 0.001$. $n = 4$. n.s.: not significantly affected. n.d.: not detected. (**m,n**) Immunohistochemical results of *in vivo* canine IVDs treated with no (control), one (1× NCM) or two (2× NCM) intradiscal injections of 50 µL of 10 mg/mL NCM (samples collected 6 months after first intradiscal injections). Representative samples of all 3 conditions (in this

case for NX-IVDs) are depicted. NX: partial NP removal to induce moderate instead of mild IVD degeneration. *: $p < 0.05$, ***: $p < 0.001$, respectively (Mann-Whitney U with Bonferroni *posthoc* test), n = 5.

a

Protein	log FC	FDR
DUSP5	5.24032	0.00000
KRT19	6.40595	0.00000
GAPDH	3.44100	0.00000
p-cJun	2.29226	0.00000
cJun	1.39165	0.00001
p-JNK/SAPK	-2.23973	0.00002
CDC2	1.18255	0.00002
p-PKC α/βII	-1.02759	0.00058
p-S6 ribosomal protein	1.67497	0.00156
p-PKC	-1.33674	0.00217
DUSP16	-1.41367	0.00234
RELB	-0.69037	0.01028
p-ERK1/2	-0.99264	0.01201
DUSP6	0.92630	0.05321
KRT18	-0.50258	0.05376
SPRED2	-0.44460	0.08392
cRaf	-0.58087	0.14435
bRaf	-0.62955	0.14680
p-MAP4K1 (HPK1)	-0.37659	0.27875
SRC	-0.39876	0.27875
PAK4	-0.41540	0.28132
Actin	-0.33708	0.29180

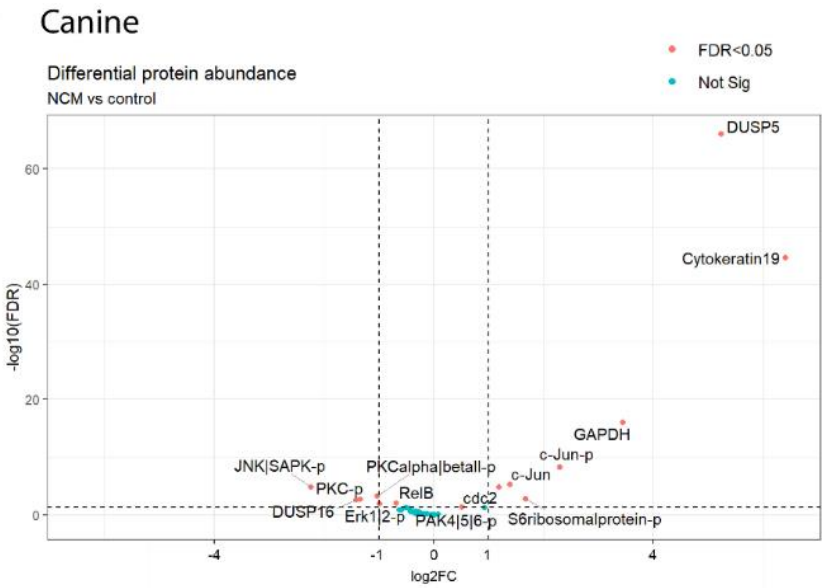

b

Protein	log FC	FDR
p-MAP4K1 (HPK1)	-5.77915	3.1e-147
PAK4	-5.43854	3.0e-126
SPRED2	-4.28431	9.8e-64
CA12	-4.72625	4.4e-52
p-PKC	-4.67287	2.7e-51
p-DUSP1	2.78525	1.9e-32
p-PKC α/β	-2.74970	2.0e-29
PAX1	-2.79173	2.9e-26
p-S6 ribosomal protein	2.40228	4.1e-21
SRC	-2.10509	4.0e-19
p-ERK1/2	-1.52822	7.4e-15
p-bRaf	-2.74346	2.4e-14
CDC2	-4.03234	5.2e-14
JAK2	-2.57813	8.4e-14
GAPDH	1.26810	1.1e-13
p-cJun	-1.77738	7.5e-13
KRT18	-1.54539	1.7e-12
FOXF1	-2.39429	5.0e-12
PAK1/2/3	1.66637	4.0e-11
Actin-β	-1.18788	1.1e-10
cJun	-1.83982	9.4e-08
α-Tubulin	0.93681	1.3e-07
DUSP5	1.12944	1.0e-06

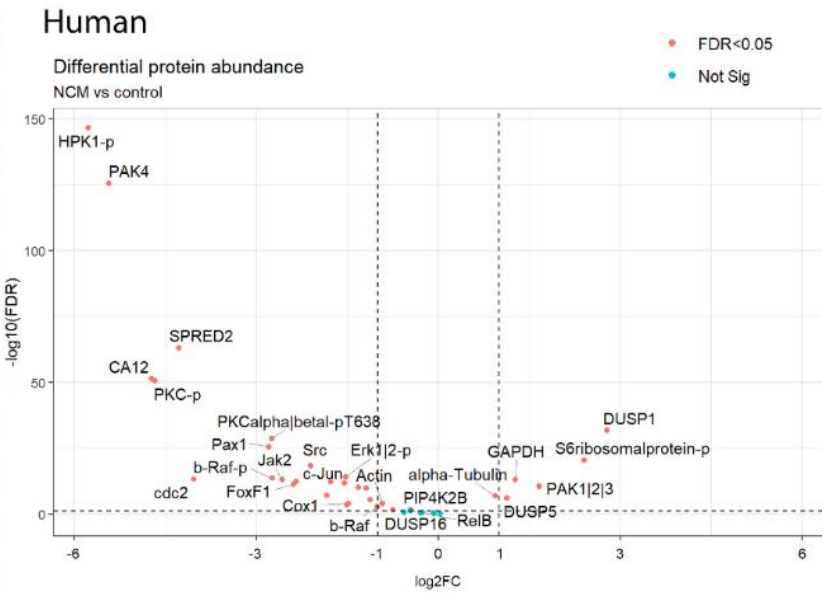

Fig. 4. Tables and volcano plots for proteins differentially expressed after NCM-treatment as determined by DigiWest technology. (**a**) Canine and (**b**) human NPCs were treated for 3 days with 10 mg/mL NCM or basal culture medium. n = 4 per species. FDR: False Discovery Rate, ERK: extracellular signal-regulated kinase, JNK/SAPK: cJun N-terminal kinase/stress-activated protein kinase, MAP4K1: Mitogen-activated protein kinase kinase kinase kinase 1 (HPK1), PKC: protein kinase C, DUSP: Dual-Specificity Phosphatase, GAPDH: Glyceraldehyde 3-phosphate dehydrogenase, CDC: cyclin-dependent kinase, KRT: cytokeratin, FOXF1: Forkhead Box F1, SPRED2: Sprouty Related EVH1 Domain Containing 2, CA12: Carbonic Anhydrase 12, PAX1: Paired Box 1, JAK2: Janus Kinase 2.

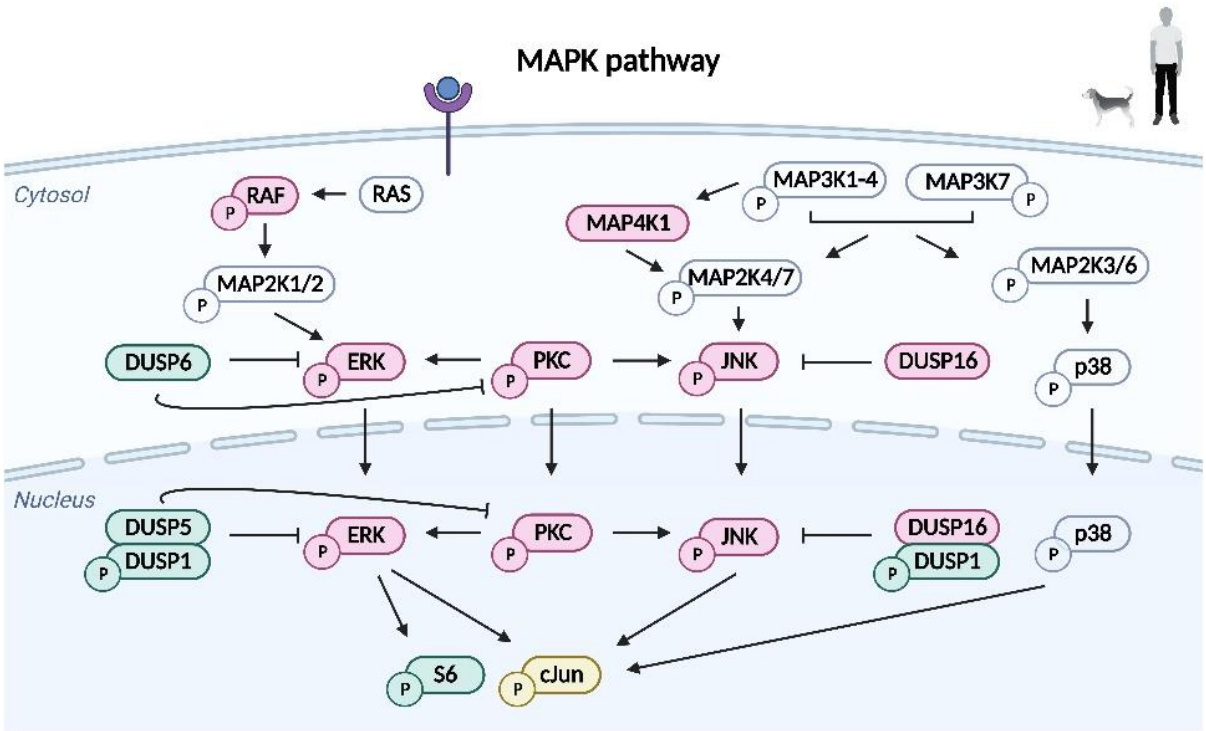

Fig. 5. Mitogen-activated protein kinase (MAPK) signaling pathway as influenced by NCM treatment in canine and human NPCs from degenerate IVDs. Red and green indicates that these signaling proteins are down- and upregulated, respectively, in NCM-treated NPCs compared with controls. Yellow: upregulated in canine, but downregulated in human NPCs. Proteins illustrated in light blue were not significantly affected by NCM treatment. This schematic picture is based on previous publications MAPK: Mitogen-activated protein kinase, MAP4K1: Mitogen-activated protein kinase kinase kinase kinase 1 (HPK1), MAP3K: Mitogen-activated protein kinase kinase kinase, MAP2K: Mitogen-activated protein kinase kinase, ERK: extracellular signal-regulated kinase, JNK/SAPK: cJun N-terminal kinase/stress-activated protein kinase, PKC: protein kinase C, DUSP: Dual-Specificity Phosphatase, S6: S6 ribosomal protein.

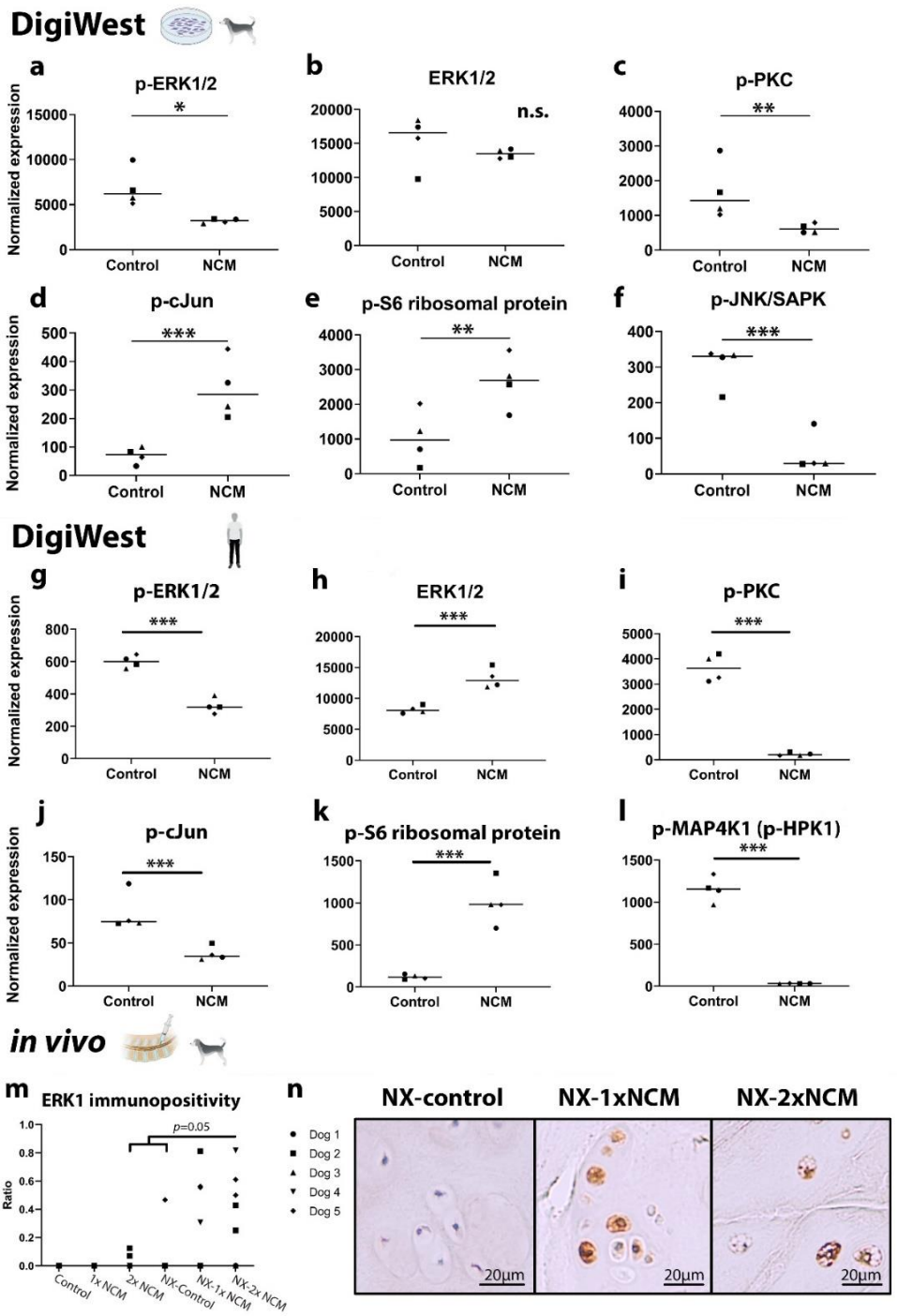

Fig. 6. NCM affects the Mitogen-activated protein kinase (MAPK) pathway in canine and human NCM-treated NPCs versus controls, as determined by DigiWest technology and in degenerated canine IVDs treated with NCM *in vivo*. (**a-l**) Canine and human NPCs were treated for 3 days with basal culture medium with/without 10 mg/mL NCM. *, **, ***: $p < 0.05$, < 0.01, and < 0.001, respectively (False Discovery Rate). $n = 4$. n.s.: not significantly affected. ERK: extracellular signal-regulated kinase, JNK/SAPK: cJun N-terminal kinase/stress-activated protein kinase, MAP4K1: Mitogen-activated protein kinase kinase kinase kinase 1 (HPK1), PKC: protein kinase C. (**m,n**) Immunohistochemical results of *in vivo* canine IVDs treated with no (control), one (1× NCM) or two (2× NCM) intradiscal injections of 50 µL of 10 mg/mL NCM (samples collected 6 months after the first intradiscal injections). Representative samples of all 3 conditions (in this case for NX-IVDs) are depicted. NX: partial NP removal to induce moderate instead of mild IVD degeneration. Mann-Whitney U with Bonferroni *posthoc* test, $n = 5$.

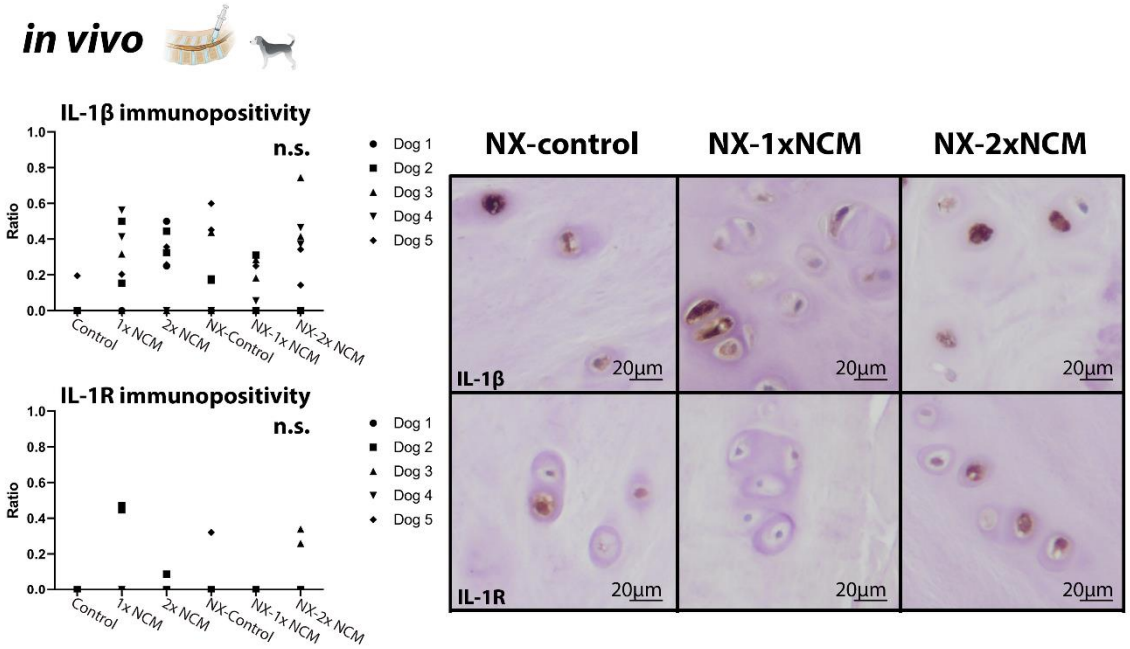

Fig. 7. IL-1β and IL-1R immunohistochemical results of *in vivo* canine IVDs treated with no (control), one (1× NCM) or two (2× NCM) intradiscal injections of 50 µL of 10 mg/mL NCM. Samples were collected 6 months after the first intradiscal injections. Representative samples of all 3 conditions (in this case for NX-IVDs) are depicted. NX: partial NP removal to induce moderate instead of mild IVD degeneration. *n* = 5. n.s.: not significantly affected.

NCM inhibits other pathways associated with pro-inflammatory mediators

NF-κB (a transcription factor involved in various biological processes, *i.e.* inflammation, immunity, differentiation, cell growth, and apoptosis) is a homo- or heterodimeric complex formed by the Rel-like domain-containing proteins RELA, RELB, NF-κB1 and NF-κB2 (Bren *et al*., 2001). Only RELB was lower expressed in NCM-treated cNPCs versus controls, but not in hNPCs (Fig. 8**c,f**). Affirmatively, pathway analysis indicated that NF-κB and Toll-like receptor cascades were inhibited by NCM (Activation of AP-1 family of transcription factors; Table 4 and 5). Also the Phospho-Phospholipase A2 (PLA2) pathway was inhibited in cNPCs treated with NCM (Table 4). The PLA2 enzymes convert phospholipids into arachidonic acid (a precursor of prostaglandins, associated with inflammation), and facilitate membrane repair and production of inflammatory lipid mediators (Leslie, 1997).

AGE receptor and RUNX2 signaling is negatively influenced by NCM

In cNPCs, but not hNPCs, advanced glycosylation end product (AGE) receptor (RAGE) signaling was negatively affected by NCM (Table 4 and 5). AGEs have been shown to increase levels of reactive-oxygen-species and promote inflammation (Illien-Junger *et al*., 2013), but can also induce osteogenic differentiation and calcification in the IVD (Illien-Jünger *et al*., 2016). In line with this, RUNX2-mediated signaling was also negatively regulated by NCM in both hNPCs and cNPCs (Table 4 and 5).

NCM may inhibit angio- and neurogenesis in cNPCs

Reactome pathway analysis indicated that NCM treatment reduced vascular endothelial growth factor (VEGF) and neurite outgrowth signaling in cNPCs (Table 4).

Cell cycle regulation is stimulated by NCM

In cNPCs, expression of Glyceraldehyde 3-phosphate dehydrogenase (GAPDH) and cell division cycle protein 2 homolog (CDC2), both involved in cell proliferation/cell cycle regulation,

were increased in NCM-treated NPCs versus controls ($p < 0.001$, Fig. 8**a,b**). In hNPCs, GAPDH expression was increased, while CDC2 expression was decreased after NCM treatment ($p < 0.001$, Fig. 8**d,e**). Furthermore, Reactome analysis of cNPCs showed that cell cycle regulation (mitosis) pathways were stimulated (Table 4). In contrast, senescence and apoptosis pathways were mainly suppressed by NCM in cNPCs, and not affected in hNPCs (Table 4 and 5).

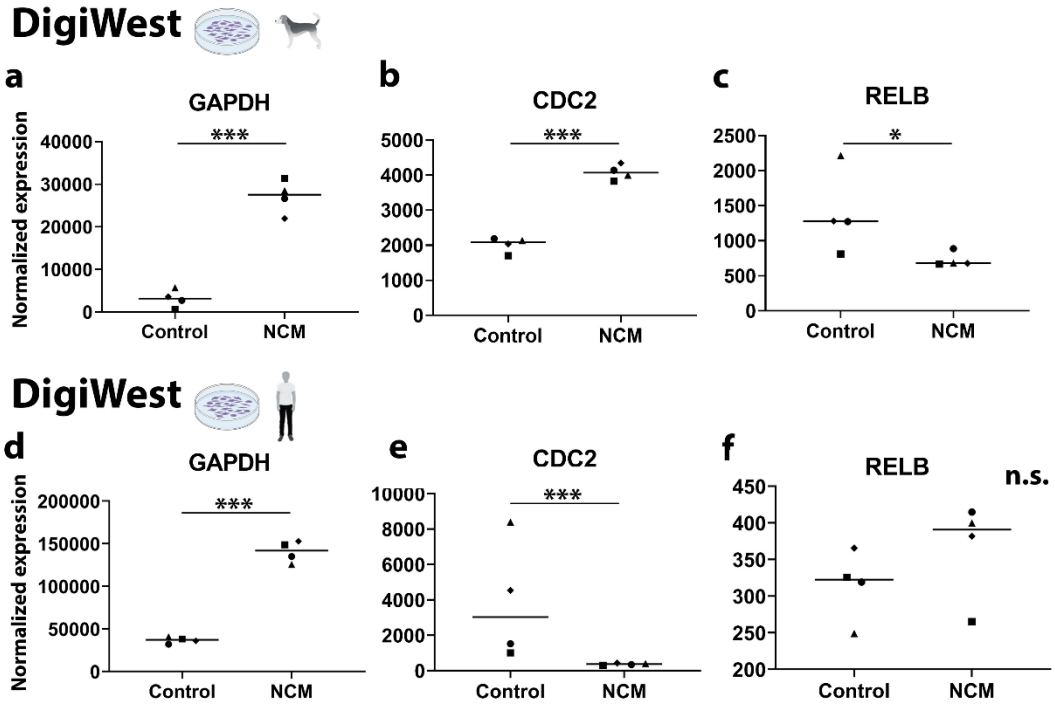

Fig. 8. NCM significantly affects cell cycle and transcription factor protein expression in canine and human NCM-treated NPCs versus controls. (**a-f**) Protein expression was determined by DigiWest technology. Canine and human NPCs were treated for 3 days with 10 mg/mL NCM or basal culture medium. *: $p < 0.05$, ***: $p < 0.001$ (False Discovery Rate). $n = 4$. n.s.: not significantly affected. GAPDH: Glyceraldehyde 3-phosphate dehydrogenase, CDC: cyclin-dependent kinase.

NCM stimulates the expression of healthy NP markers *in vivo*

DigiWest analysis of cNPCs treated for 72 hours with 10 mg/mL NCM indicated that NCM only upregulated cytokeratin 19 (KRT19) expression ($p < 0.001$), whereas the other phenotypic markers that were tested were not significantly affected by NCM (Fig. 9**a-f**). In hNPCs, KRT19 expression was upregulated by NCM treatment ($p < 0.001$, Fig. 9**i**), whereas KRT18, FOXF1, PAX1, and CA12 expression were significantly decreased in NCM-treated hNPCs ($p < 0.001$, Fig. 9**g-l**) and KRT8 expression was not detected.

According to Mann-Whitney U statistical analysis, there was a non-significant trend towards increased KRT19 expression in NC-2× NCM IVDs compared with NX-control IVDs ($p = 0.1$). In accordance with the DigiWest results, additional Chi-Square statistical analysis indicated that the number of dogs in which KRT19 was expressed in the NP was significantly higher in 2× NCM NX-IVDs compared with the control NX-IVDs ($p < 0.05$, Fig. 10**a**). In contrast to the DigiWest data, however, PAX1 and FOXF1 immunopositivity was increased in Beagle NX-IVDs treated with 2× NCM compared with NX-control IVDs ($p < 0.05$, Fig. 10**b,c**). FOXF1 immunopositivity was also increased in 2× NCM-treated noNX-IVDs when compared with control- and 1× NCM-treated noNX-IVDs ($p < 0.001$).

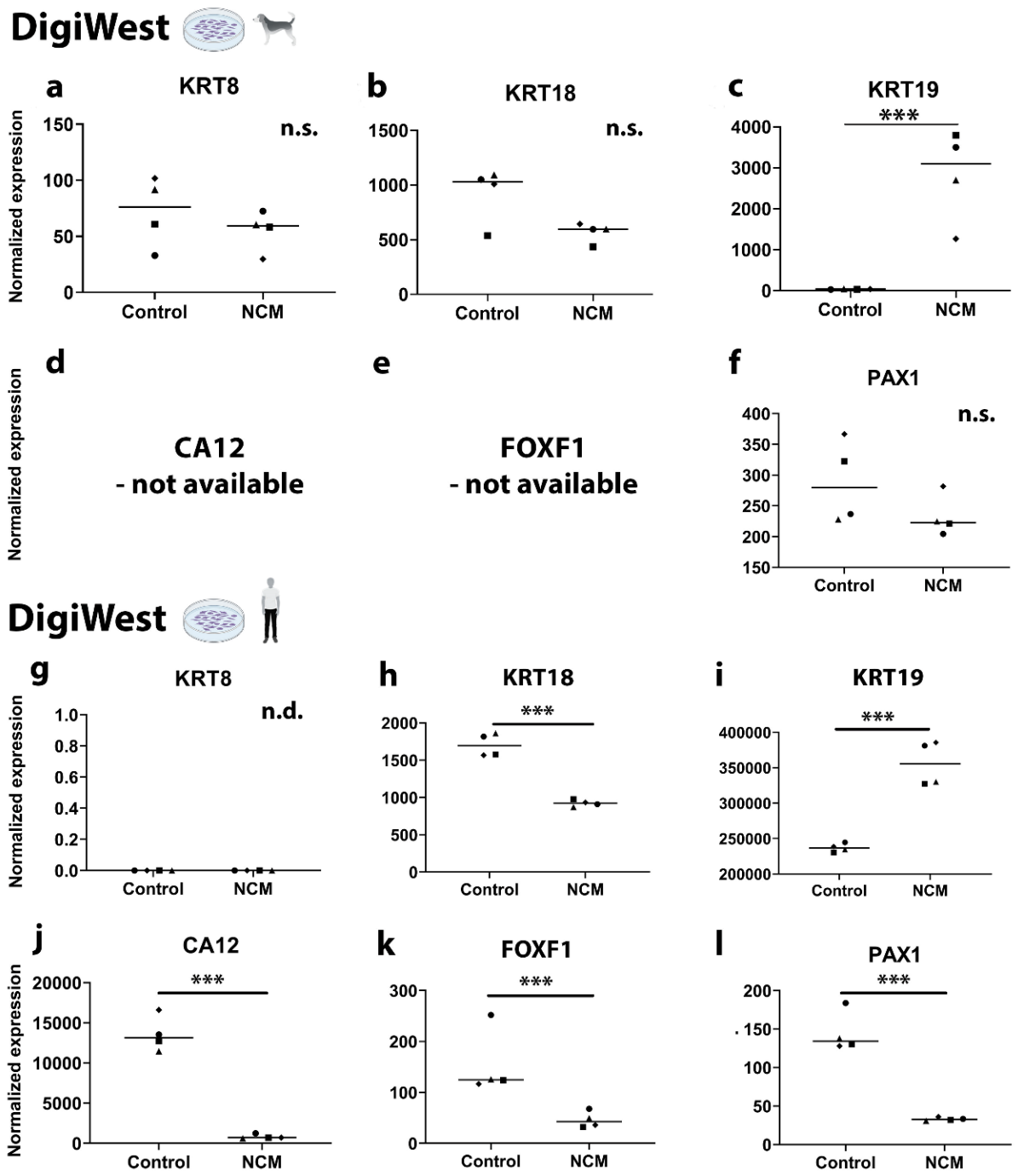

Fig. 9. NCM significantly affects NP specific marker expression in canine and human NCM-treated NPCs versus untreated controls, as determined by DigiWest technology and in degenerated canine IVDs treated with NCM *in vivo*. (**a-l**) Canine and human NPCs were treated for 3 days with basal culture medium with/without 10 mg/mL NCM. ***: $p < 0.001$ (False Discovery Rate). $n = 4$. n.s.: not significantly affected. n.d.: not detected. CA12: carbonic anhydrase 12, KRT: cytokeratin, FOXF1: Forkhead Box F1, PAX1: paired box 1.

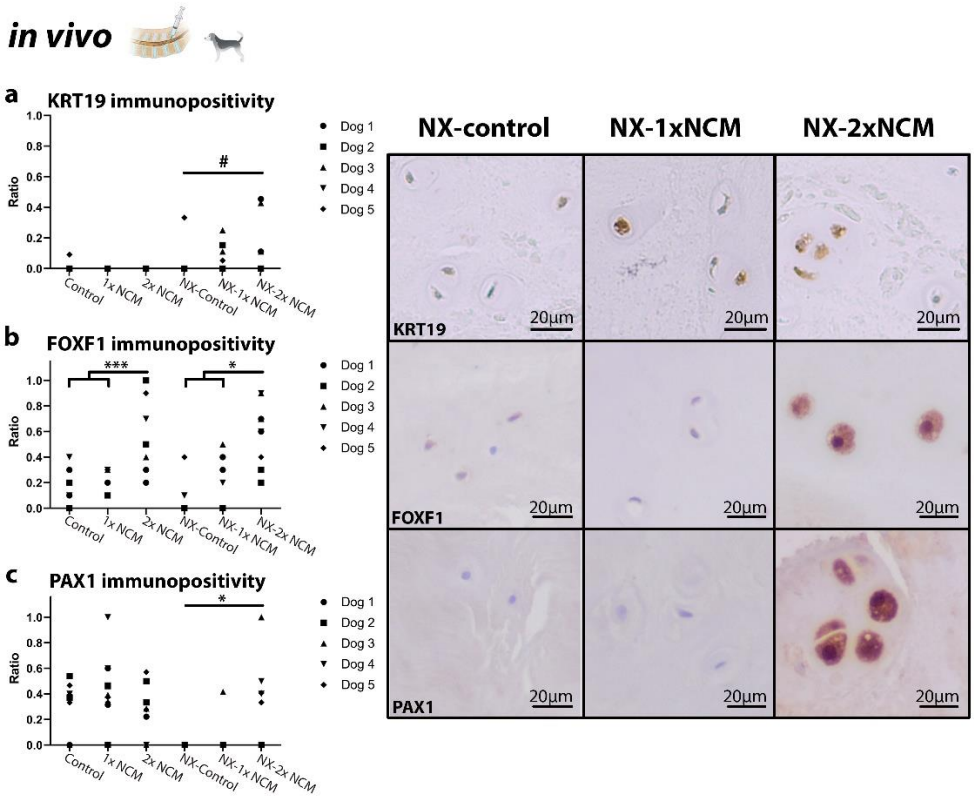

Fig. 10. Immunohistochemical results of *in vivo* canine IVDs treated with no (control), one (1× NCM) or two (2× NCM) intradiscal injections of 50 µL of 10 mg/mL NCM. Samples were collected 6 months after the first intradiscal injections. Ratio of immunopositive cells were determined for phenotypic markers (**a**) KRT19, (**b**) FOXF1, and (**c**) PAX1. Representative images of all 3 conditions (in this case for NX-IVDs) are depicted. NX: partial NP removal to induce moderate instead of mild IVD degeneration. *: $p < 0.05$, ***: $p < 0.001$ (Mann-Whitney U with Bonferroni *posthoc* test), #: $p = 0.025$ (Chi-square test); $n = 5$. KRT: cytokeratin, FOXF1: Forkhead Box F1, PAX1: paired box 1.

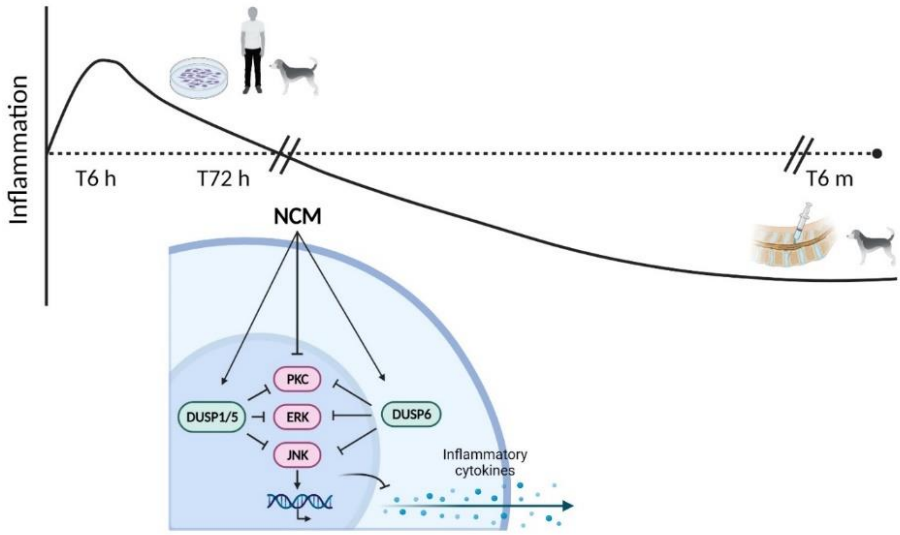

Fig. 11. Main conclusion of the current study. NCM exerts its long-term anti-inflammatory effects mainly by increasing cytosolic DUPS6 and nuclear DUSP1 and DUSP5 expression, which together dephosphorylate p-ERK1/2, p-JNK, and p-PKC (all involved in the MAPK signaling pathway) and by directly dephosphorylating p-PKC. Decreased p-ERK and p-JNK expression leads to inhibited inflammatory cytokine production.

Table 4. Reactome pathway analysis of canine NPCs treated with NCM. Head pathways (bold) and sub-pathways (non-bold) are listed together in one row. The fold enrichment of the proteins in the pathways is represented compared with expected values from the reference list. The pathways in the table indicates over-representation of this category in the analyzed list: more genes are observed than expected on the basis of the reference list (for this category, the number of genes in the list is greater than the expected value) (Mi *et al*., 2019). Pos: positively influenced pathway, Neg: negatively influenced pathway, Pos/neg: both positively and negatively regulated proteins in this pathway.

Pathway name	# genes overlap with ref list	Fold Enrichment	Pos/neg	Raw P-value	False Discovery Rate
Phospho-PLA2 pathway	1 of 2	> 100	Neg	2.18E-03	3.42E-02
Ca-dependent events	2 of 37	74.19		3.61E-04	8.11E-03
PLC beta mediated events	2 of 49	56.02		6.18E-04	1.22E-02
G-protein mediated events	2 of 54	50.84		7.45E-04	1.44E-02
Opioid Signalling	2 of 90	30.50		1.99E-03	3.21E-02
Disinhibition of SNARE formation	2 of 5	> 100	Neg	1.04E-05	9.57E-04
Platelet activation, signaling and aggregation	4 of 260	21.12		3.22E-05	1.82E-03
Negative feedback regulation of MAPK pathway	2 of 6	> 100	Pos/neg	1.38E-05	1.15E-03
Negative regulation of MAPK pathway	4 of 42	> 100		2.91E-08	1.45E-05
RAF/MAP kinase cascade	4 of 264	23.97		3.41E-05	1.89E-03
MAPK1/MAPK3 signaling	5 of 269	29.33		1.08E-06	1.42E-04
MAPK family signaling cascades	6 of 308	30.22		5.33E-08	2.21E-05
Phosphorylation of proteins involved in the G2/M transition by Cyclin A:Cdc2 complexes	1 of 3	> 100	Pos	2.91E-03	4.42E-02
Cell Cycle, Mitotic	4 of 517	10.62		4.42E-04	9.42E-03
Activation of the AP-1 family of transcription factors	3 of 10	> 100	Neg	8.89E-08	2.46E-05
MAPK targets/ Nuclear events mediated by MAP kinases	3 of 31	> 100		1.84E-06	2.19E-04
MAP kinase activation	3 of 63	65.36		1.39E-05	1.12E-03
TRAF6 mediated induction of NF-κB and MAP kinases upon TLR7/8 or 9 activation	3 of 89	46.27		3.77E-05	2.00E-03
MyD88 dependent cascade initiated on endosome	3 of 90	45.75		3.89E-05	1.90E-03

Toll Like Receptor 9 (TLR9) Cascade	3 of 94	43.81		4.42E-05	2.00E-03
Toll-like Receptor Cascades	3 of 154	26.74		1.85E-04	5.23E-03
Toll Like Receptor 7/8 (TLR7/8) Cascade	3 of 91	45.25		4.02E-05	1.93E-03
MyD88:MAL(TIRAP) cascade initiated on plasma membrane	3 of 100	41.18		5.28E-05	2.03E-03
Toll Like Receptor TLR1:TLR2 Cascade	3 of 103	39.98		5.76E-05	2.11E-03
Toll Like Receptor 2 (TLR2) Cascade	3 of 103	39.98		5.76E-05	2.14E-03
Toll Like Receptor TLR6:TLR2 Cascade	3 of 100	41.18		5.28E-05	2.00E-03
Toll Like Receptor 4 (TLR4) Cascade	3 of 132	31.2		1.18E-04	3.78E-03
Toll Like Receptor 3 (TLR3) Cascade	3 of 92	44.76		4.15E-05	1.92E-03
TRIF(TICAM1)-mediated TLR4 signaling	3 of 96	42.89		4.69E-05	2.09E-03
MyD88-independent TLR4 cascade	3 of 96	42.89		4.69E-05	2.05E-03
Interleukin-17 signaling	3 of 71	58.00		1.96E-05	1.40E-03
Cytokine Signaling in Immune system	4 of 697	7.88		1.34E-03	2.34E-03
MyD88 cascade initiated on plasma membrane	3 of 84	49.02		3.19E-05	1.99E-03
Toll Like Receptor 10 (TLR10) Cascade	3 of 84	49.02		3.19E-05	1.89E-03
Toll Like Receptor 5 (TLR5) Cascade	3 of 84	49.02		3.19E-05	1.94E-03
Apoptosis	2 of 7	> 100	Neg	1.78E-05	1.38E-03
RSK activation	2 of 7	> 100		1.78E-05	1.34E-03
CREB1 phosphorylation through NMDA receptor-mediated activation of RAS signaling	2 of 27	> 100		1.99E-04	5.27E-03
Post NMDA receptor activation events	2 of 77	35.36	Neg	1.48E-03	2.49E-02
Activation of NMDA receptors and postsynaptic events	2 of 90	30.5		1.99E-03	3.23E-02
Neurotransmitter receptors and postsynaptic signal transmission	4 of 197	27.87		1.10E-05	9.82E-04
Transmission across Chemical Synapses	4 of 260	21.12		3.22E-05	1.87E-03
Depolymerisation of the Nuclear Lamina	3 of 13	> 100		1.74E-07	4.33E-05
Nuclear Envelope Breakdown	3 of 47	87.61	Pos/neg	5.99E-06	6.50E-04
Mitotic Prophase	4 of 104	52.79		9.32E-07	1.29E-04
M Phase	4 of 375	14.64		1.31E-04	4.13E-03
Activation of RAC1	3 of 13	> 100		1.74E-07	3.94E-05
Signaling by ROBO receptors	5 of 215	31.92	Pos	3.65E-07	6.07E-05
Axon guidance	7 of 549	17.5		5.35E-08	1.91E-05

Nervous system development	7 of 574	16.74		7.23E-08	2.25E-05
Signal attenuation	2 of 9	> 100	Neg	2.71E-05	1.83E-03
Insulin receptor signaling cascade	2 of 45	61.00		5.25E-04	1.10E-02
Signaling by Insulin receptor	2 of 69	39.79		1.19E-03	2.13E-02
Signaling by Receptor Tyrosine Kinases	4 of 505	10.87		4.05E-04	8.85E-03
MAPK3 (ERK1) activation	2 of 9	> 100	Neg	2.71E-05	1.88E-03
RAF-independent MAPK1/3 activation	5 of 22	> 100		7.77E-12	1.94E-08
Gastrin-CREB signaling pathway via PKC and MAPK	3 of 16	> 100	Neg	3.00E-07	5.35E-05
G alpha (q) signaling events	3 of 214	19.24		4.77E-04	1.01E-02
Regulation of the apoptosome activity	2 of 11	> 100	Neg	3.84E-05	1.99E-03
Formation of apoptosome	2 of 11	> 100		3.84E-05	1.95E-03
Cytochrome c-mediated apoptotic response	2 of 13	> 100		5.17E-05	2.04E-03
Apoptotic factor-mediated response	2 of 18	> 100		9.33E-05	3.06E-03
Intrinsic Pathway for Apoptosis	2 of 52	52.79		6.93E-04	1.35E-02
Frs2-mediated activation	2 of 11	> 100	Neg	3.84E-05	1.92E-03
Prolonged ERK activation events	2 of 14	> 100		5.90E-05	2.13E-03
Signaling to ERKs	2 of 31	88.55		2.58E-04	6.49E-03
Signaling by NTRK1 (TRKA)	2 of 112	24.51		3.04E-03	4.57E-02
RHO GTPases Activate NADPH Oxidases	4 of 24	> 100	Neg	3.68E-09	3.06E-06
RHO GTPase Effectors	4 of 288	19.06		4.77E-05	2.05E-03
Signaling by Rho GTPases	7 of 670	14.34		2.05E-07	4.26E-05
Advanced glycosylation end product receptor signaling	2 of 13	> 100	Neg	5.17E-05	2.01E-03
Trafficking of GluR2-containing AMPA receptors	2 of 13	> 100	Neg	5.17E-05	2.11E-03
Trafficking of AMPA receptors	2 of 27	> 100		1.99E-04	5.32E-03
Glutamate binding, activation of AMPA receptors and synaptic plasticity	2 of 27	> 100		1.99E-04	5.38E-03
ERKs are inactivated	2 of 13	> 100	Pos/neg	5.17E-05	2.08E-03
ERK/MAPK targets	2 of 22	> 100		1.35E-04	4.16E-03
Nuclear Events (kinase and transcription factor activation)	2 of 61	45.00		9.42E-04	1.75E-02
Golgi Cisternae Pericentriolar Stack Reorganization	2 of 13	> 100	Pos/neg	5.17E-05	2.15E-03
Spry regulation of FGF signaling	2 of 14	> 100	Neg	5.90E-05	2.10E-03

Negative regulation of FGFR1 signaling	2 of 26	> 100		1.85E-04	5.12E-03
Signaling by FGFR1	2 of 41	66.96		4.39E-04	9.44E-03
Signaling by FGFR2	2 of 76	36.12		1.44E-03	2.44E-02
Negative regulation of FGFR2 signaling	2 of 28	98.04		2.13E-04	5.52E-03
Signaling by FGFR2	2 of 65	42.23		1.06E-03	1.94E-02
Negative regulation of FGFR4 signaling	2 of 27	> 100		1.99E-04	5.21E-03
Signaling by FGFR4	2 of 35	78.43		3.25E-04	7.56E-03
Negative regulation of FGFR3 signaling	2 of 23	> 100		1.47E-04	4.47E-03
Signaling by FGFR3	2 of 32	85.79		2.74E-04	6.669E-03
WNT5A-dependent internalization of FZD4	2 of 15	> 100	Neg	6.69E-05	2.28E-03
PCP/CE pathway	2 of 91	30.17		2.04E-03	3.26E-02
VEGFR2 mediated cell proliferation	2 of 16	> 100	Neg	7.52E-05	2.53E-03
VEGFA-VEGFR2 Pathway	2 of 94	29.20		2.17E-03	3.42E-02
Signaling by VEGF	2 of 104	26.40		2.64E-03	4.03E-02
Signal transduction by L1	2 of 20	> 100	Neg	1.13E-04	3.71E-03
RUNX2 regulates osteoblast differentiation	2 of 23	> 100	Neg	1.47E-04	4.31E-03
RUNX2 regulates bone development	2 of 30	91.51		2.42E-04	6.16E-03
Transcriptional regulation by RUNX2	3 of 117	35.19		8.33E-05	2.77E-03
Growth hormone receptor signaling	2 of 23	> 100	Neg	1.47E-04	4.41E-03
Estrogen-dependent nuclear events downstream of ESR-membrane signaling	2 of 24	> 100	Neg	1.59E-04	4.61E-03
Extra-nuclear estrogen signaling	2 of 73	37.61		1.33E-03	2.34E-02
ESR-mediated signaling	3 of 187	22.02		3.24E-04	7.68E-03
Signaling by Nuclear Receptors	3 of 261	15.78		8.44E-04	1.61E-02
Thrombin signalling through proteinase activated receptors (PARs)	2 of 31	88.55	Neg	2.58E-04	6.43E-03
Oncogene Induced Senescence	2 of 33	83.19	Neg	2.90E-04	7.03E-03
Cellular Senescence	3 of 164	25.11		2.22E-04	5.69E-03
Cellular responses to stress	4 of 718	7.65		1.50E-03	2.51E-02
RHO GTPases Activate WASPs and WAVEs	2 of 35	78.43	Neg	3.25E-04	7.43E-03
MAP2K and MAPK activation	2 of 39	70.39	Neg	3.99E-04	8.80E-03
Regulation of PTEN gene transcription	3 of 59	69.79	Pos/neg	1.15E-05	9.89E-04

PTEN Regulation	3 of 137	30.06		1.32E-04	4.10E-03
PIP3 activates AKT signaling	3 of 251	16.41		7.55E-04	1.45E-02
Intracellular signaling by second messengers	4 of 291	18.87		4.96E-05	2.10E-03
Senescence-Associated Secretory Phenotype (SASP)	3 of 81	50.84	Pos/neg	2.87E-05	1.88E-03
NCAM signaling for neurite out-growth	2 of 59	46.53	Neg	8.83E-04	1.67E-02
FCERI mediated MAPK activation	3 of 89	46.27	Pos/neg	3.77E-05	2.04E-03
Fc epsilon receptor (FCERI) signaling	3 of 187	22.02		3.24E-04	7.61E-03
Oxidative Stress Induced Senescence	3 of 92	44.76	Pos/neg	4.15E-05	1.95E-03
MAPK6/MAPK4 signaling (JUN, CDC2)	2 of 88	31.20	Pos	1.91E-03	3.11E-02
PI5P, PP2A and IER3 Regulate PI3K/AKT Signaling	2 of 92	29.84	Neg	2.08E-03	3.30E-02
Negative regulation of the PI3K/AKT network	2 of 99	27.73		2.40E-03	3.71E-02

Table 5. Reactome pathway analysis of human NPCs treated with NCM. Head pathways (bold) and sub-pathways (non-bold) are listed together in one row. The fold enrichment of the proteins in the pathways is represented compared with expected values from the reference list. The pathways in the table indicates over-representation of this category in the analyzed list: more genes are observed than expected on the basis of the reference list (for this category, the number of genes in the list is greater than the expected value) (Mi et al., 2019). Pos: positively influenced pathway, Neg: negatively influenced pathway, Pos/neg: both positively and negatively regulated proteins in this pathway.

Pathway name	# genes overlap with ref list	Fold Enrichment	+/-	raw P value	FDR
Negative feedback regulation of MAPK pathway	2 of 6	> 100	Pos/neg	2.50E-05	2.39E-03
Negative regulation of MAPK pathway	4 of 42	98.04		1.03E-07	1.60E-05
RAF/MAP kinase cascade	8 of 264	31.20		9.12E-11	5.69E-08
MAPK3 (ERK1) activation	3 of 9	> 100	Neg	1.71E-07	2.51E-05
RAF-independent MAPK1/3 activation	5 of 22	> 100		3.99E-11	3.31E-08
MAPK1/MAPK3 signaling	9 of 269	34.44		1.92E-12	2.39E-09
MAPK family signaling cascades	10 of 308	33.42		1.07E-13	2.67E-10

Activation of the AP-1 family of transcription factors	2 of 10	> 100	Neg	5.87E-05	4.57E-03
MAPK targets/ Nuclear events mediated by MAP kinases	2 of 31	66.42		4.64E-04	1.99E-02
Frs2-mediated activation	2 of 11	> 100	Neg	6.93E-05	4.94E-03
Prolonged ERK activation events	2 of 14	> 100		1.06E-04	6.99E-03
Signaling to ERKs	2 of 31	66.42		4.64E-04	2.03E-02
Signaling by NTRKs	3 of 131	23.58		2.83E-04	1.41E-02
Signaling by Receptor Tyrosine Kinases	7 of 505	14.27		3.28E-07	4.55E-05
Depolymerisation of the Nuclear Lamina	2 of 13	> 100	Neg	9.32E-05	6.46E-03
Nuclear Envelope Breakdown	2 of 47	43.81		1.02E-03	3.65E-02
Cell Cycle, Mitotic	4 of 517	7.96		1.42E-03	4.65E-02
Spry regulation of FGF signaling	2 of 14	> 100	Neg	1.06E-04	6.81E-03
Negative regulation of FGFR1 signaling	2 of 26	79.19		3.33E-04	1.60E-02
Signaling by FGFR1	3 of 41	75.33		1.01E-05	1.09E-03
Signaling by FGFR	3 of 76	40.64		5.90E-05	4.45E-03
Negative regulation of FGFR2 signaling	2 of 28	73.53		3.83E-04	1.74E-02
Negative regulation of FGFR4 signaling	2 of 27	76.26		3.58E-04	1.68E-02
Signaling by FGFR4	2 of 35	58.83		5.84E-04	2.27E-02
Negative regulation of FGFR3 signaling	2 of 23	89.52		2.65E-04	1.40E-02
Signaling by FGFR3	2 of 32	64.34		4.93E-04	2.01E-02
Gastrin-CREB signalling pathway via PKC and MAPK	2 of 16	> 100	Neg	1.36E-04	8.25E-03
RAF activation	3 of 33	93.59	Neg	5.47E-06	6.20E-04
Paradoxial activation of RAF signaling by kinase inactive BRAF	5 of 45	>100	Neg	1.03E-09	3.22E-07
Signaling by RAF1 mutants	5 of 40	>100	Neg	5.97E-10	2.48E-07
Oncogenic MAPK signaling	6 of 82	75.33		1.88E-10	9.39E-08
Diseases of signal transduction	7 of 418	17.24		9.28E-08	1.54E-05
Signaling by moderate kinase activity BRAF mutants	4 of 35	>100	Neg	5.19E-08	9.95E-06
Signaling downstream of RAS mutants	5 of 45	>100	Neg	1.03E-09	3.68E-07
Signaling by RAS mutants	5 of 45	>100		1.03E-09	2.86E-07
RUNX2 regulates osteoblast differentiation	2 of 23	89.52	Neg	2.65E-04	1.35E-02
RUNX2 regulates bone development	2 of 30	68.63		4.36E-04	1.94E-02

Transcriptional regulation by RUNX2	3 of 117	26.40		2.04E-04	1.13E-02
Growth hormone receptor signaling	2 of 23	89.52	Neg	2.65E-04	1.38E-02
Signaling by high-kinase activity BRAF mutants	4 of 35	>100	Neg	5.19E-08	9.95E-06
RHO GTPases Activate NADPH Oxidases	2 of 24	85.79	Neg	2.87E-04	1.40E-02
MAP2K and MAPK activation	4 of 39	>100	Neg	7.77E-08	1.38E-05
Signaling by BRAF and RAF fusions	5 of 64	80.43	Neg	5.41E-09	1.12E-06
Signaling by SCF-KIT	2 of 39	52.79	Neg	7.17E-04	2.67E-02
Signaling by ERBB2	2 of 46	44.76	Neg	9.83E-04	3.55E-02
Post NMDA receptor activation events	3 of 77	40.11	Pos/neg	6.12E-05	4.49E-03
Activation of NMDA receptors and postsynaptic events	3 of 90	34.31		9.59E-05	6.46E-03
Neurotransmitter receptors and postsynaptic signal transmission	4 of 197	20.90		3.76E-05	3.13E-03
Transmission across Chemical Synapses	4 of 260	15.84		1.08E-04	6.67E-03
Signaling by ROBO receptors	4 of 215	19.15	Pos/Neg	5.26E-05	4.23E-03
ESR-mediated signaling	3 of 187	16.52	Neg	7.83E-04	2.87E-02
Intracellular signaling by second messengers	4 of 291	14.15	Neg	1.66E-04	9.64E-03
Infectious disease	7 of 895	8.05	Pos/neg	1.41E-05	1.41E-03

Discussion

The aim of this study was to determine the mode of action of porcine NCM in the degenerative IVD environment. Our findings demonstrate that porcine NCM induces an initial inflammatory response, but thereafter exerts a prolonged anti-inflammatory effect mainly by influencing the MAPK pathway. This was confirmed at the IVD level in a dog model where disc degeneration was induced by partial nuclectomy (Bach *et al*., 2018). Furthermore, based on the pathway analysis of differential protein expression upon NCM treatment in canine and human NPCs, new hypotheses involved in the instructive capacity of NCM are indicated.

NCM initially induces pro-inflammatory mediators in native NPCs

In previous work, prolonged anti-inflammatory effects of porcine NCM were shown *in vitro* in bovine NPCs cultured for 28 days (Schmitz *et al*., 2022; De Vries *et al*., 2015) and *in vivo* in dog IVDs treated with NCM for 6 months (Bach *et al*., 2018). Interestingly, the current study shows that NCM induced an initial inflammatory response in canine and human NPCs and that this response was mediated at least in part by activated NF-κB signaling. This could be due to fragmented cell-free (porcine) DNA remnants in NCM, which are known to cause inflammation (Motwani *et al*., 2019; Poli *et al*., 2017), *e.g.* in chronic diseases like osteoarthritis (Nagata *et al*., 2010). Additionally, ECM fragments could act as danger-associated molecular patterns (DAMPs) (Lees *et al*., 2015; Schaefer, 2014), which can activate amongst others toll-like receptors (TLRs). Human IVD cells are known to express TLRs (Klawitter *et al*., 2014) and their activation has been implicated to induce IVD degeneration (Krock *et al*., 2017). An initial inflammatory response may, however, when properly balanced, contribute to tissue repair/regeneration (Molinos *et al*., 2015; Sun *et al*., 2013) and might thus have favorable effects at the long-term.

NCM inhibits pro-inflammatory mediators by affecting the MAPK pathway

After 72 hours, the initial NCM-mediated inflammatory response gradually dissolved. At this timepoint, NCM mainly affected MAPK signaling in canine and human NPCs, by decreasing p-ERK/p-JNK/p-PKC expression via increased DUSP1/5/6 levels. The latter was confirmed *in vivo* in 6-months-treated canine IVDs. p-ERK1/2 immunopositivity was absent in all *in vivo* samples, which most probably is related to extensive period of fixation followed by months of decalcification not allowing for appropriate immunohistochemical analysis of phosphorylated proteins (Wolf *et al*., 2014). This study additionally indicated that the inflammation-related PLA2 and NF-κB cascades (downstream of the MAPK pathway) (Bren *et al*., 2001; Tian *et al*., 2018; Wang *et al*., 2017b) were inhibited by NCM. Since these pathways are known to be involved in production and release of pro-inflammatory mediators in degenerated IVDs (Daniels *et al*., 2017; Ni *et al*., 2019), these findings could well explain the anti-inflammatory effects of NCM. Furthermore, others also showed that inhibiting MAPK signaling could reduce the catabolic effects of inflammatory mediators in the IVD (Park *et al*., 2016; Sun *et al*., 2020).

NCM inhibits also other pathways associated with pro-inflammatory mediators

The current study indicates that NCM also inhibited RAGE signaling, which is in line with our previous study with indications that NCM prevented AGE accumulation *in vivo* (Bach *et al*., 2018). AGEs have also been shown to induce osteogenic differentiation and calcification in the IVD (Illien-Jünger *et al*., 2016; Svenja *et al*., 2015). Interestingly, together with RAGE signaling, the RUNX2 signaling was also inhibited by NCM, indicating that it might prevent disc hypertrophy/calcification, processes that can occur during advanced stages of IVD degeneration (Rutges *et al*., 2010).

Angio- (Capossela *et al*., 2018) and neurogenesis (Navone *et al*., 2012) are other processes involved in advanced IVD degeneration. According to Reactome pathway analysis, NCM suppressed, and neurite outgrowth. Interestingly, NC-conditioned medium (NCCM) has previously been shown to exert both anti- (Cornejo *et al*., 2015) and pro-angiogenic (de Vries *et al*., 2018a) effects, whereas NCM did not affect vessel growth (de Vries *et al*.,

2018a). Furthermore, NCCM inhibited neurite growth in one study (Purmessur *et al*., 2015), whereas another study showed that NCCM and NCM both increased neurite expressing cell numbers (de Vries *et al*., 2018a). In our previous *in vivo* study, no indications for increased *VEGF* expression, nerve or vessel ingrowth were present after six months of NCM treatment (Bach *et al*., 2018). Nonetheless, future studies that test NCM-based regenerative strategies *in vivo* should carefully assess the risk of angio- and neurogenesis during a prolonged time period.

NCM affects the expression of proteins involved in cell cycle regulation and proliferation

In previous work, it was established that NCM increased cell proliferation *in vitro* (Bach *et al*., 2018; de Vries *et al*., 2019). DigiWest analysis shed light on the possible mechanisms behind this effect of NCM. The ERK/JNK-MAPK signaling pathway is, besides involved in inflammation, also involved in cell cycle regulation, by promoting and/or inhibiting proliferation and apoptosis, dependent on the specific context (cell type, stimulus, pathologic status) (Cagnol and Chambard, 2010; Guma and Firestein, 2012; Mi *et al*., 2018). Although expression of key proteins (p-ERK/p-JNK/p-PKC) of the MAPK pathway was inhibited by NCM, p-S6 levels were increased. p-S6 is involved in the regulation of amongst others cell size and proliferation (Ruvinsky *et al*., 2009; Ruvinsky and Meyuhas, 2006), but it also stimulates cartilage repair (Zhang *et al*., 2020). P-S6 can, besides by ERK/JNK-MAPK, also be activated by other pathways, *e.g.* mammalian target of rapamycin (mTOR), which is in turn activated by amongst others certain growth factors (Hay and Sonenberg, 2004). Therefore, the increased p-S6 levels in NCM-treated NPCs, possibly caused by the growth factors present in NCM (Bach *et al*., 2022), might facilitate cell proliferation possibly facilitating an anabolic response.

Regulation of cJun, which is involved in cell cycle regulation and proliferation, is complex (Wisdom *et al*., 1999) and depends on the activation period (Guma and Firestein, 2012). Our study showed decreased p-cJun expression in hNPCs, but increased p-cJun levels in cNPCs treated with NCM. This may be explained by cJun being reported to induce cell cycle progression and inhibit apoptosis by distinct mechanisms; cJun-mediated G1 progression is independent of serine 63/73 phosphorylation, whereas inhibition of apoptosis requires serines 63/73 (Wisdom *et al*., 1999). Thus, in the canine NPCs cJun could have been increased because cell proliferation was stimulated by NCM independent of specific JNK activation. Additionally, the *Fibroblast growth factor-4 (FGF4)* retrogene insertion is responsible for chondrodystrophy and IVD degeneration in dog breeds like Beagles (Brown *et al*., 2017). There are indications that FGF4 influences proliferation via c-Jun activation (Kook *et al*., 2013), and therefore, this retrogene in combination with NCM treatment could have contributed to the increased cJun expression in Beagle NPCs compared with hNPCs.

Furthermore, NCM-treated NPCs demonstrated an increased GAPDH and CDC2 expression, the latter only in cNPCs. GAPDH was initially identified as a glycolytic enzyme and considered as a housekeeping gene, but emerging evidence indicates that GAPDH is involved in diverse functions other than its role in energy metabolism, *e.g.* cell cycle regulation, proliferation and apoptosis (Carujo *et al*., 2006; Kosova *et al*., 2017; Zhang *et al*., 2015). Interestingly, GAPDH enables the activation of CDC2 (Carujo *et al*., 2006), which is also a key player in these processes (Dorée and Hunt, 2002; Haneke *et al*., 2020; Liu *et al*., 2008).

Altogether, NCM affects cell proliferation and apoptosis via different players.

NCM improves the NPC phenotype *in vivo* at the long-term follow up

NCM treatment improved the cNPC phenotype *in vivo* after 6 months, indicated by increased expression of well-known phenotypic NP markers KRT19, FOXF1, and PAX1 (Akker *et al*., 2017; Richardson *et al*., 2017). *In vitro*, only an increase in KRT19 protein expression was detected in both canine and human NPCs, whereas other phenotypic markers were downregulated in hNPCs. This discrepancy could be due to the used culture system, since it is known that NPCs don't maintain their specific morphology and phenotype in two-dimensional (monolayer) culture (Wang *et al*., 2001). Furthermore, the absence of phenotypic markers

could also be due to passage number used in the current study (P2 for cNPCs and P3 for hNPCs).

Altogether, the results from our study show that the anabolic effects and inhibition of pro-inflammatory mediators, detected after intradiscal NCM injection *in vivo* (Bach *et al*., 2018), are accompanied by an improved NPC phenotype in addition to upregulation of DUSP protein expression. A limitation of the current study is that it only focused on the NP, whereas the AF and the EPs are also known to be involved in the inflammatory process during IVD degeneration (Lai et al., 2023; Yamagishi et al., 2022).

Clinical perspective and conclusions

Further research should focus on improving the clinical applicability of NCM. Extracellular DNA containing porcine endogenous retroviruses is problematic within the NCM (Wilson, 2008), since they have been shown to infect human cells *in vitro* and thus pose a risk for patients (Martin *et al*., 2000). Also, fragmented cell-free DNA may cause inflammation (Motwani *et al*., 2019; Poli *et al*., 2017). Prior to utilization in a clinical setting, processing of the NCM to remove DNA is thus required (Schmitz *et al*., 2022).

In conclusion, NCM initially stimulated pro-inflammatory mediators *in vitro*, but thereafter exerts its effects by influencing the MAPK pathway. The latter leads to the reduced expression of inflammatory cytokines and improved NPC phenotype after prolonged treatment (Fig. 11). The work presented enhance our understanding of how NCM instructs the degenerate NPCs and provide for new hypothesis to study in NC-based therapeutic strategies employing cell-free or cell-based approaches.

Acknowledgements

The authors would like to thank Adel Medzikovic for helping with the execution of experiments. The graphical abstract, Fig. 1-3 and Fig. 5-11 were all (partly) created with BioRender.com.

Author contributions

LL, FCB, and MAT contributed to the design of the work. LL, FCB, GE, TSB, GGHvdA, TCS, CS contributed to acquisition of laboratory data. LL, FCB, FMR, TSB, GGHvdA, MAT performed data analysis. LL, FCB, FMR, CLLM, KI, LBC, MAT contributed to interpretation of the data. LL, FCB, FMR, TSB, GGHvdA, MAT drafted the article. All authors critically revised the article for intellectual content. All authors approved the final version and agree to be accountable for all aspects of the work.

Ethics approval and consent to participate

For this study, spines were collected from Beagles that had been euthanized in unrelated research studies (approved by the Utrecht University Animal Ethics Committee; Centrale Commissie Dierproeven). Furthermore, IVDs from human donors were obtained during a standard postmortem diagnostic procedure in which part of the lumbar spine was collected within 48 hours after death, as approved the Local Medical Ethical Committee number (12-364). The material was used in line with the code 'Proper Secondary Use of Human Tissue' as installed by the Federation of Biomedical Scientific Societies.

Funding

This project has received funding from the European Union's Horizon 2020 research and innovation program under grant agreement no. 825925 and the Dutch Arthritis Society (LLP22 and LLP12).

Conflict of interest

The authors declare no conflict of interest.

Supplementary material

Supplementary material associated with this article can be found, in the online version, at https://doi.org/10.22203/eCM.v046a04.

References

Akker GGH, Koenders MI, Loo FAJ, Lent PLEM, Davidson EB, Kraan PM (2017) Transcriptional profiling distinguishes inner and outer annulus fibrosus from nucleus pulposus in the bovine intervertebral disc. Eur Spine J **26**: 2053-2062. DOI: 10.1007/s00586-017-5150-3.

Bach FC, Tellegen AR, Beukers M, Miranda-Bedate A, Teunissen M, de Jong WAM, de Vries SAH, Creemers LB, Benz K, Meij BP, Ito K, Tryfonidou MA (2018) Biologic canine and human intervertebral disc repair by notochordal

cell-derived matrix: From bench towards bedside. Oncotarget **9**: 26507-26526. DOI: 10.18632/oncotarget.25476.

Bach FC, de Vries SA, Krouwels A, Creemers LB, Ito K, Meij BP, Tryfonidou MA (2015) The species-specific regenerative effects of notochordal cell-conditioned medium on chondrocyte-like cells derived from degenerated human intervertebral discs. Eur Cell Mater **30**: 132-137. DOI: 10.22203/ecm.v030a10.

Bach FC, Zhang Y, Miranda-Bedate A, Verdonschot LC, Bergknut N, Creemers LB, Ito K, Sakai D, Chan D, Meij BP, Tryfonidou MA (2016b) Increased caveolin-1 in intervertebral disc degeneration facilitates repair. Arthritis Res Ther **18**: 59. DOI: 10.1186/s13075-016-0960-y.

Bach FC, Poramba-Liyanage DW, Riemers FM, Guicheux J, Camus A, Iatridis JC, Chan D, Ito K, Le Maitre CL, Tryfonidou MA (2022) Notochordal Cell-Based Treatment Strategies and Their Potential in Intervertebral Disc Regeneration. Front Cell Dev Biol **9**: 780749. DOI: 10.3389/fcell.2021.780749.

Bren GD, Solan NJ, Miyoshi H, Pennington KN, Pobst LJ, Paya CV (2001) Transcription of the RelB gene is regulated by NF-κB. Oncogene **20**: 7722-7733. DOI: 10.1038/sj.onc.1204868.

Brown EA, Dickinson PJ, Mansour T, Sturges BK, Aguilar M, Young AE, Korff C, Lind J, Ettinger CL, Varon S, Pollard R, Brown CT, Raudsepp T, Bannasch DL (2017) FGF4 retrogene on CFA12 is responsible for chondrodystrophy and intervertebral disc disease in dogs. Proc Natl Acad Sci U S A **114**: 11476-11481. DOI: 10.1073/pnas.1709082114.

Cagnol S, Chambard JC (2010) ERK and cell death: Mechanisms of ERK-induced cell death - Apoptosis, autophagy and senescence. FEBS J **277**: 2-21. DOI: 10.1111/j.1742-4658.2009.07366.x.

Capossela S, Bertolo A, Gunasekera K, Pötzel T, Baur M, Stoyanov J V (2018) VEGF vascularization pathway in human intervertebral disc does not change during the disc degeneration process. BMC Res Notes **11**: 333. DOI: 10.1186/s13104-018-3441-3.

Cargnello M, Roux PP (2011) Activation and Function of the MAPKs and Their Substrates, the MAPK-Activated Protein Kinases. Microbiol Mol Biol Rev **75**: 50-83. DOI: 10.1128/mmbr.00031-10.

Carujo S, Estanyol JM, Ejarque A, Agell N, Bachs O, Pujol MJ (2006) Glyceraldehyde 3-phosphate dehydrogenase is a SET-binding protein and regulates cyclin B-cdk1 activity. Oncogene **25**: 4033-4042. DOI: 10.1038/sj.onc.1209433.

Chen HF, Chuang HC, Tan TH (2019) Regulation of dual-specificity phosphatase (Dusp) ubiquitination and protein stability. Int J Mol Sci **20**: 2668. DOI: 10.3390/ijms20112668.

Clark S, Horton R (2018) Low back pain: a major global challenge. Lancet **391**: 2302. DOI: 10.1016/S0140-6736(18)30725-6.

Cornejo MC, Cho SK, Giannarelli C, Iatridis JC, Purmessur D (2015) Soluble factors from the notochordal-rich intervertebral disc inhibit endothelial cell invasion and vessel formation in the presence and absence of pro-inflammatory cytokines. Osteoarthr Cartil **23**: 487-496. DOI: 10.1016/j.joca.2014.12.010.

Daniels J, Binch AAL, Le Maitre CL (2017) Inhibiting IL-1 signaling pathways to inhibit catabolic processes in disc degeneration. J Orthop Res **35**: 74-85. DOI: 10.1002/jor.23363.

Dorée M, Hunt T (2002) From Cdc2 to Cdk1: When did the cell cycle kinase join its cyclin partner? J Cell Sci **115**: 2461-2464. DOI: 10.1242/jcs.115.12.2461.

Fenton TR, Gout IT (2011) Functions and regulation of the 70 kDa ribosomal S6 kinases. Int J Biochem Cell Biol **43**: 47-59. DOI: 10.1016/j.biocel.2010.09.018.

Freemont AJ (2009) The cellular pathobiology of the degenerate intervertebral disc and discogenic back pain. Rheumatology **48**: 5-10. DOI: 10.1093/rheumatology/ken396.

Gruskin E, Doll BA, Futrell FW, Schmitz JP, Hollinger JO (2012) Demineralized bone matrix in bone repair: History and use. Adv Drug Deliv Rev **64**: 1063-1077. DOI: 10.1016/j.addr.2012.06.008.

Guma M, Firestein GS (2012) c-Jun N-Terminal Kinase in Inflammation and Rheumatic Diseases. Open Rheumatol J **6**: 220-231. DOI: 10.2174/1874312901206010220.

Haneke K, Schott J, Lindner D, Hollensen AK, Damgaard CK, Mongis C, Knop M, Palm W, Ruggieri A, Stoecklin G (2020) CDK1 couples proliferation with protein synthesis. J Cell Biol **219**: e201906147. DOI: 10.1083/jcb.201906147.

Hay N, Sonenberg N (2004) Upstream and downstream of mTOR. Genes Dev **18**: 1926-1945. DOI: 10.1101/gad.1212704.

Huang CY, Tan TH (2012) DUSPs, to MAP kinases and beyond. Cell Biosci **2**: 24. DOI: 10.1186/2045-3701-2-24.

Hunter CJ, Matyas JR, Duncan NA (2004) Cytomorphology of notochordal and chondrocytic cells from the nucleus pulposus: a species comparison. J Anat **205**: 357-362. DOI: 10.1111/j.0021-8782.2004.00352.x.

Illien-Junger S, Grosjean F, Laudier DM, Vlassara H, Striker GE, Iatridis JC (2013) Combined Anti-Inflammatory and Anti-AGE Drug Treatments Have a Protective Effect on Intervertebral Discs in Mice with Diabetes. PLoS One **8**: e64302. DOI: 10.1371/journal.pone.0064302.

Illien-Jünger S, Torre OM, Kindschuh WF, Chen X, Laudier DM, Iatridis JC (2016) AGEs induce ectopic endochondral ossification in intervertebral discs. Eur Cells Mater **32**: 257-270. DOI: 10.22203/eCM.v032a17.

Klawitter M, Hakozaki M, Kobayashi H, Krupkova O, Quero L, Ospelt C, Gay S, Hausmann O, Liebscher T, Meier U, Sekiguchi M, Konno SI, Boos N, Ferguson SJ, Wuertz K (2014) Expression and regulation of toll-like receptors (TLRs) in human intervertebral disc cells. Eur Spine J **23**: 1878-1891. DOI: 10.1007/s00586-014-3442-4.

Kook SH, Jeon YM, Lim SS, Jang MJ, Cho ES, Lee SY, Choi KC, Kim JG, Lee JC (2013) Fibroblast Growth Factor-4 Enhances Proliferation of Mouse Embryonic Stem Cells via Activation of c-Jun Signaling. PLoS One **8**: e71641. DOI: 10.1371/journal.pone.0071641.

Kosova AA, Khodyreva SN, Lavrik OI (2017) Role of glyceraldehyde-3-phosphate dehydrogenase (GAPDH) in DNA repair. Biochem **82**: 643-654. DOI: 10.1134/S0006297917060013.

Krock E, Rosenzweig DH, Currie JB, Bisson DG, Ouellet JA, Haglund L (2017) Toll-like receptor activation induces degeneration of human intervertebral discs. Sci Rep **7**: 17184. DOI: 10.1038/s41598-017-17472-1.

Lai A, Iliff D, Zaheer K, Wang D, Gansau J, Laudier DM, Zachariou V, Iatridis JC. Spinal Cord Sensitization and Spinal Inflammation from an In Vivo Rat Endplate Injury Associated with Painful Intervertebral Disc Degeneration. International Journal of Molecular Sciences. 2023; 24(4):3425. https://doi.org/10.3390/ijms24043425.

Lees S, Golub SB, Last K, Zeng W, Jackson DC, Sutton P, Fosang AJ (2015) Bioactivity in an aggrecan 32-mer fragment is mediated via toll-like receptor 2. Arthritis Rheumatol **67**: 1240-1249. DOI: 10.1002/art.39063.

Leslie CC (1997) Properties and regulation of cytosolic phospholipase A2. J Biol Chem **272**: 16709-16712. DOI: 10.1074/jbc.272.27.16709.

Li L, Zhao GD, Shi Z, Qi LL, Zhou LY, Fu ZX (2016) The Ras/Raf/MEK/ERK signaling pathway and its role in the occurrence and development of HCC (Review). Oncol Lett **12**: 3045-3050. DOI: 10.3892/ol.2016.5110.

Liu P, Kao TP, Huang H (2008) CDK1 promotes cell proliferation and survival via phosphorylation and inhibition of FOXO1 transcription factor. Oncogene **27**: 4733-4744. DOI: 10.1038/onc.2008.104.

Le Maitre CL, Freemont AJ, Hoyland JA (2005) The role of interleukin-1 in the pathogenesis of human intervertebral disc degeneration. Arthritis Res Ther **7**: R732-R745. DOI: 10.1186/ar1732.

Martin U, Winkler ME, Id M, Radeke H, Arseniev L, Takeuchi Y, Simon AR, Patience C, Haverich A, Steinhoff G (2000) Productive infection of primary human endothelial cells by pig endogenous retrovirus (PERV). Xenotransplantation **7**: 138-142. DOI: 10.1034/j.1399-3089.2000.00052.x.

Mi D, Cai C, Zhou B, Liu X, Ma P, Shen S, Lu W, Huangy W (2018) Long non-coding RNA FAF1 promotes intervertebral disc degeneration by targeting the Erk signaling pathway. Mol Med Rep **17**: 3158-3163. DOI: 10.3892/mmr.2017.8237.

Mi H, Muruganujan A, Huang X, Ebert D, Mills C, Guo X, Thomas PD (2019) Protocol Update for large-scale genome and gene function analysis with the PANTHER classification system (v.14.0). Nat Protoc **14**: 703-721. DOI: 10.1038/s41596-019-0128-8.

Molinos M, Almeida CR, Caldeira J, Cunha C, Gonçalves RM, Barbosa MA (2015) Inflammation in intervertebral disc degeneration and regeneration. J R Soc Interface **12**: 20150429. DOI: 10.1098/rsif.2015.0429.

Motwani M, Pesiridis S, Fitzgerald KA (2019) DNA sensing by the cGAS–STING pathway in health and disease. Nat Rev Genet **20**: 657-674. DOI: 10.1038/s41576-019-0151-1.

Nagata S, Hanayama R, Kawane K (2010) Autoimmunity and the Clearance of Dead Cells. Cell **140**: 619-630. DOI: 10.1016/j.cell.2010.02.014.

Nakashima S (2002) Protein kinase C alpha (PKC alpha): regulation and biological function. J Biochem **132**: 669-675. DOI: 10.1093/oxfordjournals.jbchem.a003272.

Navone SE, Marfia G, Canzi L, Ciusani E, Canazza A, Visintini S, Campanella R, Parati EA (2012) Expression of neural and neurotrophic markers in nucleus pulposus cells isolated from degenerated intervertebral disc. J Orthop Res **30**: 1470-1477. DOI: 10.1002/jor.22098.

Neefjes M, Housmans BAC, van den Akker GGH, van Rhijn LW, Welting TJM, van der Kraan PM (2021) Reporter gene comparison demonstrates interference of complex body fluids with secreted luciferase activity. Sci Rep **11**: 1359. DOI: 10.1038/s41598-020-80451-6.

Ni L, Zheng Y, Gong T, Xiu C, Li K, Saijilafu, Li B, Yang H, Chen J (2019) Proinflammatory macrophages promote degenerative phenotypes in rat nucleus pulpous cells partly through ERK and JNK signaling. J Cell Physiol **234**: 5362-5371. DOI: 10.1002/jcp.27507.

Nishina H, Wada T, Katada T (2004) Physiological roles of SAPK/JNK signaling pathway. J Biochem **136**: 123-126. DOI: 10.1093/jb/mvh117.

Lopez-Bergami P, Huang C, Goydos JS, Yip D, Bar-Eli M, Herlyn M, Smalley KS, Mahale A, Eroshkin A, Aaronson S, Ronai Z (2007) Rewired ERK-JNK signaling pathways in melanoma. Cancer Cell **11**: 447-460. DOI: 10.1016/j.ccr.2007.03.009.

Park JJ, Moon HJ, Park JH, Kwon TH, Park YK, Kim JH (2016) Induction of proinflammatory cytokine production in intervertebral disc cells by macrophage-like THP-1 cells requires mitogen-activated protein kinase activity. J Neurosurg Spine **24**: 167-175. DOI: 10.3171/2015.3.SPINE14729.

Pietrzak WS, Dow M, Gomez J, Soulvie M, Tsiagalis G (2012) The *in vitro* elution of BMP-7 from demineralized bone matrix. Cell Tissue Bank **13**: 653-661. DOI: 10.1007/s10561-011-9286-9.

Poli C, Augusto JF, Dauvé J, Adam C, Preisser L, Larochette V, Pignon P, Savina A, Blanchard S, Subra JF, Chevailler A, Procaccio V, Croué A, Créminon C, Morel A, Delneste Y, Fickenscher H, Jeannin P (2017) IL-26 Confers Proinflammatory Properties to Extracellular DNA. J Immunol **198**: 3650-3661. DOI: 10.4049/jimmunol.1600594.

Purmessur D, Cornejo MC, Cho SK, Roughley PJ, Linhardt RJ, Hecht AC, Iatridis JC (2015) Intact glycosaminoglycans from intervertebral disc-derived notochordal cell-conditioned media inhibit neurite growth while maintaining neuronal cell viability. Spine J **15**: 1060-1069. DOI: 10.1016/j.spinee.2015.02.003.

Richardson SM, Ludwinski FE, Gnanalingham KK, Atkinson RA, Freemont AJ, Hoyland JA (2017) Notochordal and nucleus pulposus marker expression is maintained by sub-populations of adult human nucleus pulposus cells through aging and degeneration. Sci Rep **7**: 1501. DOI: 10.1038/s41598-017-01567-w.

Rutges JP, Duit RA, Kummer JA, Oner FC, van Rijen MH, Verbout AJ, Castelein RM, Dhert WJ, Creemers LB (2010) Hypertrophic differentiation and calcification during intervertebral disc degeneration. Osteoarthr Cartil **18**: 1487-1495. DOI: 10.1016/j.joca.2010.08.006.

Ruvinsky I, Katz M, Dreazen A, Gielchinsky Y, Saada A, Freedman N, Mishani E, Zimmerman G, Kasir J, Meyuhas O (2009) Mice deficient in ribosomal protein S6 phosphorylation suffer from muscle weakness that reflects a growth defect and energy deficit. PLoS One **4**: e5618. DOI: 10.1371/journal.pone.0005618.

Ruvinsky I, Meyuhas O (2006) Ribosomal protein S6 phosphorylation: from protein synthesis to cell size. Trends Biochem Sci **31**: 342-348. DOI: 10.1016/j.tibs.2006.04.003.

Schaefer L (2014) Complexity of danger: The diverse nature of damage-associated molecular patterns. J Biol Chem **289**: 35237-35245. DOI: 10.1074/jbc.R114.619304.

Schmitz TC, Van Doeselaar M, Tryfonidou MA, Ito K (2022) Detergent-Free Decellularization of Notochordal Cell-Derived Matrix Yields a Regenerative, Injectable, and Swellable Biomaterial. ACS Biomater Sci Eng **8**: 3912-3923. DOI: 10.1021/acsbiomaterials.2c00790.

Sun Y, Shi X, Peng X, Li Y, Ma H, Li D, Cao X (2020) MicroRNA-181a exerts anti-inflammatory effects via inhibition of the ERK pathway in mice with intervertebral disc degeneration. J Cell Physiol **235**: 2676-2686. DOI: 10.1002/jcp.29171.

Sun Z, Zhang M, Zhao XH, Liu ZH, Gao Y, Samartzis D, Wang HQ, Luo ZJ (2013) Immune cascades in human intervertebral disc: The pros and cons. Int J Clin Exp Pathol **6**: 1009-1014.

Svenja IJ, Young L, Sheeraz AQ, Andrew CH, Weijing C, Helen V, Gary ES, James CI (2015) Chronic ingestion of advanced Glycation end products induces degenerative spinal changes and hypertrophy in aging Pre-diabetic mice. PLoS One **10**: e0116625. DOI: 10.1371/journal.pone.0116625.

Tian Z, Ma X, Yasen M, Mauck RL, Qin L, Shofer FS, Smith LJ, Pacifici M, Enomoto-Iwamoto M, Zhang Y (2018) Intervertebral Disc Degeneration in a Percutaneous Mouse Tail Injury Model. Am J Phys Med Rehabil **97**: 170-177. DOI: 10.1097/PHM.0000000000000818.

Treindl F, Ruprecht B, Beiter Y, Schultz S, Döttinger A, Staebler A, Joos TO, Kling S, Poetz O, Fehm T, Neubauer H, Kuster B, Templin MF (2016) A bead-based western for high-throughput cellular signal transduction analyses. Nat Commun **7**: 12852. DOI: 10.1038/ncomms12852.

Vergroesen PP, Kingma I, Emanuel KS, Hoogendoorn RJ, Welting TJ, van Royen BJ, van Dieën JH, Smit TH (2015) Mechanics and biology in intervertebral disc degeneration: a vicious circle. Osteoarthritis Cartilage **23**: 1057-1070. DOI: 10.1016/j.joca.2015.03.028.

De Vries SAH, Potier E, van Doeselaar M, Meij BP, Tryfonidou MA, Ito K (2015) Conditioned medium derived from notochordal cell-rich nucleus pulposus tissue stimulates matrix production by canine nucleus pulposus cells and bone marrow-derived stromal cells. Tissue Eng Part A **21**: 1077-1084. DOI: 10.1089/ten.TEA.2014.0309.

de Vries SAH, van Doeselaar M, Meij BP, Tryfonidou MA, Ito K (2018a) Notochordal cell matrix: An inhibitor of neurite and blood vessel growth? J Orthop Res **36**: 3188-3195. DOI: 10.1002/jor.24114.

de Vries S, Doeselaar MV, Meij B, Tryfonidou M, Ito K (2019) Notochordal Cell Matrix As a Therapeutic Agent for Intervertebral Disc Regeneration. Tissue Eng Part A **25**: 830-841. DOI: 10.1089/ten.TEA.2018.0026.

Wang C, Yu X, Yan Y, Yang W, Zhang S, Xiang Y, Zhang J, Wang W (2017a) Tumor necrosis factor-α: A key contributor to intervertebral disc degeneration. Acta Biochim Biophys Sin (Shanghai) **49**: 1-13. DOI: 10.1093/abbs/gmw112.

Wang J, Huang J, Wang L, Chen C, Yang D, Jin M, Bai C, Song Y (2017b) Urban particulate matter triggers lung inflammation via the ROS-MAPK- NF-κB signaling pathway. J Thorac Dis **9**: 4398-4412. DOI: 10.21037/jtd.2017.09.135.

Wang JY, Baer AE, Kraus VB, Setton LA (2001) Intervertebral disc cells exhibit differences in gene expression in alginate and monolayer culture. Spine **26**: 1747-1752. DOI: 10.1097/00007632-200108150-00003.

Williams RJ, Laagland LT, Bach FC, Ward L. Chan W, Tam V, Medzikovic A, Basavat S, Paillat L, Vedrenne N, Snuggs JW, Poramba-Liyanage DW, Hoyland JA, Chan D, Camus A, Richardson SM, Tryfonidou MA, Le Maitre CL (2023) Recommendations for intervertebral disc notochordal cell investigation: from isolation to characterisation. JOR spine e1272. DOI: 10.1002/jsp2.1272.

Wilson CA (2008) Endogenous retroviruses: Porcine endogenous retroviruses and xenotransplantation. Cell Mol Life Sci **65**: 3399-3412. DOI: 10.1007/s00018-008-8498-z.

Wisdom R, Johnson RS, Moore C (1999) c-Jun regulates cell cycle progression and apoptosis by distinct mechanisms. EMBO J **18**: 188-197. DOI: 10.1093/emboj/18.1.188.

Wolf C, Jarutat T, Vega Harring S, Haupt K, Babitzki G, Bader S, David K, Juhl H, Arbogast S (2014) Determination of phosphorylated proteins in tissue specimens requires high-quality samples collected under stringent conditions. Histopathology **64**: 431-444. DOI: 10.1111/his.12268.

Yamagishi A, Nakajima H, Kokubo Y, Yamamoto Y, Matsumine A. Polarization of infiltrating macrophages in the outer annulus fibrosus layer associated with the process of intervertebral disc degeneration and neural ingrowth in the human cervical spine. Spine J. 2022;22(5):877-886. doi:10.1016/j.spinee.2021.12.005

Zhang JY, Zhang F, Hong CQ, Giuliano AE, Cui XJ, Zhou GJ, Zhang GJ, Cui YK (2015) Critical protein GAPDH and its regulatory mechanisms in cancer cells. Cancer Biol Med **12**: 10-22. DOI: 10.7497/j.issn.2095-3941.2014.0019.

Zhang S, Hamid MR, Wang T, Liao J, Wen L, Zhou Y, Wei P, Zou X, Chen G, Chen J, Zhou G

(2020) RSK-3 promotes cartilage regeneration via interacting with rpS6 in cartilage stem/progenitor cells. Theranostics **10**: 6915-6927. DOI: 10.7150/thno.44875.

Editor's note: The Scientific Editor responsible for this paper was Sibylle Grad.